ASD-TDR-63-361

N-63-4-3

41

INVESTIGATION OF THE DISTRIBUTION OF TENSION IN NOTCHED CONSTRUCTION ELEMENTS

TECHNICAL DOCUMENTARY REPORT NO. ASD-TDR-63-361

May 1963

Directorate of Materials and Processes
Aeronautical Systems Division
Air Force Systems Command
Wright-Patterson Air Force Base, Ohio

Project No. 7351, Task No. 735106

(Prepared under Contract No. AF 61(052)-200
by the Technische Hochschule, Munchen, Germany;
Dr.-Ing. H. Neuber, author).

NOTICES

When Government drawings, specifications, or other data are used for any purpose other than in connection with a definitely related Government procurement operation, the United States Government thereby incurs no responsibility nor any obligation whatsoever; and the fact that the Government may have formulated, furnished, or in any way supplied the said drawings, specifications, or other data, is not to be regarded by implication or otherwise as in any manner licensing the holder or any other person or corporation, or conveying any rights or permission to manufacture, use, or sell any patented invention that may in any way be related thereto.

Qualified requesters may obtain copies of this report from the Armed Services Technical Information Agency, (ASTIA), Arlington Hall Station, Arlington 12, Virginia.

This report has been released to the Office of Technical Services, U.S. Department of Commerce, Washington 25, D.C., in stock quantities for sale to the general public.

Copies of this report should not be returned to the Aeronautical Systems Division unless return is required by security considerations, contractual obligations, or notice on a specific document.

33-818C, 600, 6-24-63

FOREWORD

This report was prepared by Professor Dr. Ing. H. Neuber at the Institute für Technische Mechanik, Institute of Technology, Munich, Germany under AF Contract 61(052)-200. This contract was initiated under Project 7351, "Metallic Materials", Task No. 735106 "Behavior of Metals". The work was administered under the direction of the Directorate of Materials and Processes, Aeronautical Systems Division with Dr. J. A. Herzog acting as project engineer. This report covers the investigations conducted in previous years.

The author wishes to express his appreciation to Dr. J. A. Herzog, to Capt. C. C. La Plante and Capt. D. E. Beitsch both of the European Office for Aerospace Research, Brussels, Belgium for their support and cooperation, as well as his coworkers for their help.

ABSTRACT

The theoretical part of the research work concerns a new treatment of stress- and strain concentrations for a special non-linear deformation law for shear. A relation is obtained by which the real notch stress can be evaluated from the nominal stress and the elastic stress concentration factor. The notch-angle is exactly taken into account.

The experimental part contai ıs static and fatigue tests with variously notched specimens. The strain-measurements were performed by electrical strain gages; additional measurements were made by means of the photoelastic stress-coat method. The aim of the static tests was die investigation of the notch-angle influence on the elastic stress concentration factor for tension and bending, the determination of the stress- and strain distribution in the elastic and plastic range respectively, and also the dependence of the stress concentration factor on the nominal stress for the materials used (Steel St.00.12, St.00.21, Aluminum alloy "Velodur"). The result of the fatigue tests was the establishment of Wöhler-curves for two different specimen shapes (bars with central holes) and their comparison with the Wöhler-curve of the corresponding unnotched specimen.

This technical documentary report has been reviewed and is approved.

W. G. RAMKE
Actg. Chief, Advanced Metallurgical Studies Branch
Metals and Ceramics Laboratory
Directorate of Materials and Processes

TABLE OF CONTENTS

GLOSSARY OF SYMBOLS

α	stress concentration factor in the linear (Hookian) range (ESCF)
ϱ	radius of curvature of the notch
ω	notch-angle
τ, σ	shear stress, normal stress
τ^*	parameter with dimension of stress
τ_N, σ_N	nominal stress (corresponding to the minimum section)
τ_i	maximum stress in the linear theory
τ_{MAX}, σ_{MAX}	real stress in the notch (notch stress in the non-linear theory)
ε	strain
γ	shear deformation
E	Young's modulus
G	shear modulus
$F(\tau)$	deformation law
$N(\tau)$	certain function of stress
x, y	orthogonal cartesian coordinates
u, v	orthogonal curvilinear coordinates
h_u, h_v	metric factors

(All other symbols are explained in the text)

LIST OF ILLUSTRATIONS

LIST OF ILLUSTRATIONS (CONT'D)

LIST OF ILLUSTRATIONS (CONT'D)

LIST OF ILLUSTRATIONS (CONT'D)

I. THEORETICAL PART

A new treatment of stress- and strain-concentrations in the non-linear range for shear

1. Introduction

The following treatment of the notch effect in the non-linear range for pure shear is based on the deformation law

$$G\gamma = \frac{\tau}{\sqrt{1-(\tau/\tau^*)^2}} \equiv F(\tau) \qquad (1)$$

The aim of the investigations is to determine for a given nominal stress τ_N the stress τ_{MAX} and deformation γ_{MAX} in the notch ground.

In the linear range there exists the relation

$$\tau_i = \alpha \tau_N ,$$

where α is the stress concentration factor in the elastic range (ESCF). The hypothesis is established that for the non-linear range an analogously built relation exists, but with a certain function of the stresses instead of the stresses themselves. For this function which has to satisfy certain conditions we take the expression $N(\tau)$ defined below in section 3, equation (28). Hence we have

$$N(\tau_{MAX}) = \alpha \cdot N(\tau_N) . \qquad (2)$$

Manuscript released by the author April 1960 for publication as an ASD Technical Documentary Report.

The practical procedure is shown in Fig.1 where the function $N(\tau)$ as well as the deformation law (1) are plotted. Starting from the nominal stress τ_N one gets the corresponding value of $N(\tau_N)$; this multiplied by α gives the value $\alpha N(\tau_N)$ and with the $N(\tau)$ -curve the corresponding notch stress τ_{MAX} . The deformation γ_{MAX} related herewith can be found by means of the stress-deformation curve $F(\tau)$ (cf.the arrows in Fig.1)

2. <u>Relation between Hookian stress τ_i and real stress τ_{MAX} for small nominal-stresses τ_N and large ESCF α (for arbitrary notch-angles)</u>

In his book [2] the author showed that in the limit-case of vanishing nominal stress for the deformation law (1) there exists the same relation between Hookian notch-stress τ_i and real notch-stress τ_{MAX} for flat as well as for deep notches. Arbitrary large notch-stresses with small nominal stresses are only possible for great values of the ESCF i.e. for notches with very small radius of curvature. In [2] sharply curved elliptic and hyperbolic notch-shapes had been investigated. The notch-angle influence which had hitherto not been considered will now be taken into account.

For sharply curved notches with arbitrary notch-angle ω a conformal representation is available which is given by

$$\frac{z}{i} = \frac{1}{2n+1}\left(\frac{w}{i}\right)^{2n+1} i \qquad \frac{dz}{dw} = \left(\frac{w}{i}\right)^{2n} \tag{3}$$

with $z = x+iy$; $\quad w = u+iv$; $\quad n = \frac{1}{2}\left(1-\frac{\omega}{\pi}\right)$; $\quad i = \sqrt{-1}$

By eq.(3) the half-plane $\mathrm{Im}\, w \geq 0$ is mapped into the angle region as shown in Fig.2. For the linear range (Hooke's law) the curves v = const represent the stress-lines and the curves u = const the lines of constant warping respectively.

The metric factor h in the notch-ground (i.e. for u = o, $v = v_o$) becomes

$$h_o = \left(\frac{dz}{dw}\right)_{\substack{u=o \\ v=v_o}} = v_o^{2n} \tag{4}$$

and for the radius of curvature of the notch follows

$$\frac{1}{\varrho} = \frac{1}{h_o^2}\left(\frac{\partial h}{\partial v}\right)_o = 2n\left(\frac{1}{h_o}\right)^{\frac{2n+1}{2n}} \tag{5}$$

The Hookian notch stress τ_i corresponding to the conformal representation (3) is evaluated by

$$\tau_i = \frac{B}{h_o} = B\left(\frac{1}{2n\varrho}\right)^{\frac{2n}{2n+1}} \tag{6}$$

where B is a constant.
The stress-distribution along the y-axis (x = o, u = o) can be obtained on behalf of $y = v^{2n+1}/2n+1$ and $h = v^{2n}$ from $\tau = B/h$. It follows

$$\tau = B\left[\frac{1}{(2n+1)y}\right]^{\frac{2n}{2n+1}}$$

For a notch with $\omega = 60^\circ$ this is also plotted in Fig.2 (dashed curve).

If a material is considered which obeys the non-linear deformation law (1), one gets by substitution of

$$\tau = \frac{G}{h_v} \qquad \text{and} \qquad \gamma = \frac{1}{h_u} \tag{7}$$

(cf. [2], section X; h_u and h_v are metric factors)
in eq.(1)

$$\left.\begin{aligned} &\frac{1}{h_u} = \frac{1}{\sqrt{h_v^2 - (G/\tau^*)^2}} \\ \text{or} \qquad &h_v^2 - h_u^2 = 4k \end{aligned}\right\} \tag{8}$$

with

$$k = \frac{G^2}{4\tau^{*2}} \tag{9}$$

From the first equation (7) and eq.(9) immediately follows

$$\frac{\tau}{\tau^*} = \frac{2\sqrt{k}}{h_v} \tag{10}$$

By introducing

$$h = \tfrac{1}{2}(h_u + h_v) \tag{11}$$

one obtains from eq.(8)

$$h_u = h - \frac{k}{h} \qquad \text{and} \qquad h_v = h + \frac{k}{h} \tag{12}$$

and hence with eq.(10)

$$\frac{\tau}{\tau^*} = \frac{2}{\frac{h}{\sqrt{k}} + \frac{\sqrt{k}}{h}} \tag{13}$$

Since always $\tau < \tau^*$ it is required that $h \gtrsim \sqrt{k}$. For $h \gg \sqrt{k}$ eq.(13) gives $\tau \ll \tau^*$ (slight loading) and from eq.(12) follows $h_u = h_v = h$.

If one denotes by φ the angle between the x- and u-lines in the x,y-plane there follow under consideration of the orthogonality of the u- and v-lines the relations

$$\cos\varphi = \frac{1}{h_u}\cdot\frac{\partial x}{\partial u} = \frac{1}{h_v}\frac{\partial y}{\partial v}$$

$$\sin\varphi = -\frac{1}{h_v}\frac{\partial x}{\partial v} = \frac{1}{h_u}\frac{\partial y}{\partial u}$$

and hence, using eq.(12)

$$\left.\begin{aligned} \frac{\partial x}{\partial u} &= \left(h - \frac{k}{h}\right)\cos\varphi; & \frac{\partial x}{\partial v} &= -\left(h + \frac{k}{h}\right)\sin\varphi \\ \frac{\partial y}{\partial u} &= \left(h - \frac{k}{h}\right)\sin\varphi; & \frac{\partial y}{\partial v} &= \left(h + \frac{k}{h}\right)\cos\varphi \end{aligned}\right\} \qquad (14)$$

As in [2] p. 193 is shown, $\ln h$ is a harmonic function in the u,v-system and corresponds to a conformal mapping of the u,v-plane into a fictive x_0, y_0-plane($z_0 = x_0 + iy_0$). The connection of the z_0-plane with the real body plane (z-system) is given by

$$z = z_0 - k\int \frac{d\bar{w}}{\frac{d\bar{z}_0}{d\bar{w}}} + D \qquad (15)$$

where

$$\bar{w} = u - iv; \quad \bar{z}_0 = x_0 - iy_0$$

D an unessential constant.

The metric belonging to z_0 is determined by the expression factor

$$h = \left|\frac{dz_0}{dw}\right|$$

The radius of curvature ρ can be evaluated from

$$\frac{1}{\rho} = \left|\frac{1}{h_u h_v}\cdot\frac{\partial h_u}{\partial v}\right|_{\substack{u=\sigma \\ v=v_0}} \qquad (16)$$

It follows from eq. (12)

$$dh_u = dh\left(1 + \frac{k}{h^2}\right) = \frac{h_v}{h}\, dh$$

and herewith eq.(16) yields

$$\frac{1}{s} = \left| \frac{1}{h_u h} \cdot \frac{\partial h}{\partial v} \right|_{\substack{u=o \\ v=v_o}} \tag{17}$$

For the representation function $z_o(w)$ one has in the case of the sharply curved deep notch

$$\left(\frac{dz_o}{dw}\right)^{\frac{1}{2n}} - \left(\frac{k}{\frac{dz_o}{dw}}\right)^{\frac{1}{2n}} = \frac{w}{i} \tag{18}$$

Herewith is $dz/dw = h \cdot e^{i\varphi}$, where φ means the tangent angle to the u,v-net in the z_o-plane as well as in the real (z-)plane, and one obtains with w = u + iv from eq.(18)

$$u = -\left[h^{\frac{1}{2n}} + \left(\frac{k}{h}\right)^{\frac{1}{2n}}\right] \sin\frac{\varphi}{2n}; \qquad v = \left[h^{\frac{1}{2n}} - \left(\frac{k}{h}\right)^{\frac{1}{2n}}\right] \cos\frac{\varphi}{2n} \tag{19}$$

and by differentiating

$$\left.\begin{aligned} \frac{\partial u}{\partial h} &= -\frac{1}{2nh}\left[h^{\frac{1}{2n}} - \left(\frac{k}{h}\right)^{\frac{1}{2n}}\right] \sin\frac{\varphi}{2n}; & \frac{\partial u}{\partial \varphi} &= -\frac{1}{2n}\left[h^{\frac{1}{2n}} + \left(\frac{k}{h}\right)^{\frac{1}{2n}}\right] \cos\frac{\varphi}{2n} \\ \frac{\partial v}{\partial h} &= \frac{1}{2nh}\left[h^{\frac{1}{2n}} + \left(\frac{k}{h}\right)^{\frac{1}{2n}}\right] \cos\frac{\varphi}{2n}; & \frac{\partial v}{\partial \varphi} &= -\frac{1}{2n}\left[h^{\frac{1}{2n}} - \left(\frac{k}{h}\right)^{\frac{1}{2n}}\right] \sin\frac{\varphi}{2n} \end{aligned}\right\} \tag{20}$$

It can be seen that the external edge line (v = 0) is mapped by $\varphi = \pm n\pi$ i.e. a broken line of straight curves (Fig.3). For u = o there follows φ = o, i.e. the y-axis.

There is

$$v = h^{\frac{1}{2n}} - \left(\frac{h}{h_0}\right)^{\frac{1}{2n}} \tag{21}$$

The curvature in the notch-ground must be evaluated by eq. (17). In connection with eq.(21) and the first of equations (12) follows

$$\frac{1}{\varrho} = \frac{1}{h_0 - \frac{h}{h_0}} \cdot \frac{2n}{h_0^{\frac{1}{2n}} + \left(\frac{h}{h_0}\right)^{\frac{1}{2n}}} \tag{22}$$

According eq.(11) with eq.(7) and eq.(8) there is

$$h_0 = \frac{G}{2\tau_{MAX}} \cdot \left(\sqrt{1 - \left(\frac{\tau_{MAX}}{\tau^*}\right)^2} + 1\right)$$

and with eq.(12)

$$\frac{h}{h_0} = \frac{G}{2\tau_{MAX}} \left(1 - \sqrt{1 - \left(\frac{\tau_{MAX}}{\tau^*}\right)^2}\right)$$

Hence eq.(22) becomes

$$\frac{1}{2n\varrho} = \frac{\left(\frac{\tau_{MAX}}{G}\right)^{\frac{2n+1}{2n}}}{\sqrt{1 - \left(\frac{\tau_{MAX}}{\tau^*}\right)^2} \cdot \left[\left(\frac{1}{2} + \frac{1}{2}\sqrt{1 - \left(\frac{\tau_{MAX}}{\tau^*}\right)^2}\right)^{\frac{1}{2n}} + \left(\frac{1}{2} - \frac{1}{2}\sqrt{1 - \left(\frac{\tau_{MAX}}{\tau^*}\right)^2}\right)^{\frac{1}{2n}}\right]} \tag{23}$$

On the other hand for the <u>linear (Hookian) loading-range</u> one obtains (cf. eq.(6))

$$\frac{1}{2n\varrho} = \left(\frac{\tau_i}{B}\right)^{\frac{2n+1}{2n}} \tag{24}$$

By eliminating ϱ from equations (23) and (24) there follows the relation between the notch stress τ_i for Hooke's law and the notch stress τ_{MAX} for the non-linear

law (1) which is valid for <u>small nominal stresses τ_N</u> only:

$$\tau_i = \frac{\tau_{MAX}}{\left\{\sqrt{1-\left(\frac{\tau_{MAX}}{\tau^*}\right)^2}\left[\left(\frac{1}{2}+\frac{1}{2}\sqrt{1-\left(\frac{\tau_{MAX}}{\tau^*}\right)^2}\right)^{\frac{\pi}{\pi-\omega}}+\left(\frac{1}{2}-\frac{1}{2}\sqrt{1-\left(\frac{\tau_{MAX}}{\tau^*}\right)^2}\right)^{\frac{\pi}{\pi-\omega}}\right]\right\}^{\frac{\pi-\omega}{2\pi-\omega}}} \qquad (25)$$

where $2n = 1 - \frac{\omega}{\pi}$ and B = G had been taken. The latter follows from the condition $\tau_{MAX} \to \tau_i$ for small values of τ_{MAX}.

In order to investigate the pattern of the stress-lines in the neighbourhood of a notch with straight flanks it is useful to consider the quantities h and φ as parameters. Then it follows

$$\left.\begin{aligned} \frac{\partial x}{\partial h} &= \frac{\partial x}{\partial u}\frac{\partial u}{\partial h}+\frac{\partial x}{\partial v}\frac{\partial v}{\partial h}; & \frac{\partial x}{\partial \varphi} &= \frac{\partial x}{\partial u}\frac{\partial u}{\partial \varphi}+\frac{\partial x}{\partial v}\frac{\partial v}{\partial \varphi}; \\ \frac{\partial y}{\partial h} &= \frac{\partial y}{\partial u}\frac{\partial u}{\partial h}+\frac{\partial y}{\partial v}\frac{\partial v}{\partial h}; & \frac{\partial y}{\partial \varphi} &= \frac{\partial y}{\partial u}\frac{\partial u}{\partial \varphi}+\frac{\partial y}{\partial v}\frac{\partial v}{\partial \varphi} \end{aligned}\right\} \qquad (26)$$

and in connection with equations (14) and (20)

$$\frac{\partial x}{\partial h} = -\frac{1}{2nh}\left[h^{\frac{2n+1}{2n}}+\left(\frac{b}{h}\right)^{\frac{2n+1}{2n}}\right]\sin\frac{2n+1}{2n}\varphi+\frac{b}{2nh}\left[h^{\frac{1-2n}{2n}}+\left(\frac{b}{h}\right)^{\frac{1-2n}{2n}}\right]\sin\frac{1-2n}{2n}\varphi$$

$$\frac{\partial x}{\partial \varphi} = -\frac{1}{2n}\left[h^{\frac{2n+1}{2n}}-\left(\frac{b}{h}\right)^{\frac{2n+1}{2n}}\right]\cos\frac{2n+1}{2n}\varphi+\frac{b}{2n}\left[h^{\frac{1-2n}{2n}}-\left(\frac{b}{h}\right)^{\frac{1-2n}{2n}}\right]\cos\frac{1-2n}{2n}\varphi$$

$$\frac{\partial y}{\partial h} = \frac{1}{2nh}\left[h^{\frac{2n+1}{2n}}+\left(\frac{b}{h}\right)^{\frac{2n+1}{2n}}\right]\cos\frac{2n+1}{2n}\varphi+\frac{b}{2nh}\left[h^{\frac{1-2n}{2n}}+\left(\frac{b}{h}\right)^{\frac{1-2n}{2n}}\right]\cos\frac{1-2n}{2n}\varphi$$

$$\frac{\partial y}{\partial \varphi} = -\frac{1}{2n}\left[h^{\frac{2n+1}{2n}}-\left(\frac{b}{h}\right)^{\frac{2n+1}{2n}}\right]\sin\frac{2n+1}{2n}\varphi-\frac{b}{2n}\left[h^{\frac{1-2n}{2n}}-\left(\frac{b}{h}\right)^{\frac{1-2n}{2n}}\right]\sin\frac{1-2n}{2n}\varphi$$

The integration yields

$$\left.\begin{aligned} x &= -\frac{1}{2n+1}\left[h^{\frac{2n+1}{2n}} - \left(\frac{h}{\ell}\right)^{\frac{2n+1}{2n}}\right]\sin\frac{2n+1}{2n}\varphi + \frac{h}{1-2n}\left[h^{\frac{1-2n}{2n}} - \left(\frac{h}{\ell}\right)^{\frac{1-2n}{2n}}\right]\sin\frac{1-2n}{2n}\varphi \\ y &= \frac{1}{2n+1}\left[h^{\frac{2n+1}{2n}} - \left(\frac{h}{\ell}\right)^{\frac{2n+1}{2n}}\right]\cos\frac{2n+1}{2n}\varphi + \frac{h}{1-2n}\left[h^{\frac{1-2n}{2n}} - \left(\frac{h}{\ell}\right)^{\frac{1-2n}{2n}}\right]\cos\frac{1-2n}{2n}\varphi \end{aligned}\right\} \quad (27)$$

Herewith the Cartesian coordinates x and y are expressed in terms of the parameters h and φ , similar as the curvilinear coordinates u and v in eq.(19). From equations (19) and (27) the corresponding values x(u,v) and y(u,v) easily can be evaluated. Fig. 3 shows as an example the stress-lines v = const and the lines of constant warping u = const in the neighbourhood of a notch with $\omega = 60^{\circ}$ ($2n = \frac{2}{3}$).

3. <u>Formulation of a hypothesis for the determination of the real stress τ_{MAX} from the nominal stress τ_N and the ESCF α</u>

Eq.(25) represents the relation between the linear notch stress (for Hooke's law) τ_i and the notch stress τ_{MAX} for the non-linear law (1). This equation is derived with the assumption of very small nominal stresses τ_N and great values of the ESCF α .

For arbitrary large nominal stresses τ_N and ESCF α the right-hand side of eq.(25) will assume a value deviating from τ_i which may be called $N(\tau)$

$$N(\tau) = \frac{\tau}{\left\{\sqrt{1-\left(\frac{\tau}{\tau_{\#}}\right)^2}\cdot\left[\left(\frac{1}{2}+\frac{1}{2}\sqrt{1-\left(\frac{\tau}{\tau_{\#}}\right)^2}\right)^{\frac{\pi}{\pi-\omega}} + \left(\frac{1}{2}-\frac{1}{2}\sqrt{1-\left(\frac{\tau}{\tau_{\#}}\right)^2}\right)^{\frac{\pi}{\pi-\omega}}\right]\right\}^{\frac{\pi-\omega}{2\pi-\omega}}} \quad (28)$$

and is valid for arbitrary nominal stresses and ESCF.

The relation (28) is plotted in Fig.4 for various notch angles ω . It can be seen that the influence of the notch angle is very small. Therefore the curve for $\omega = 0°$

$$N(\tau)_{\omega=0} = \frac{\tau}{\sqrt[4]{1-\left(\frac{\tau}{\tau_F}\right)^2}} \tag{29}$$

can be used approximately for all values of ω .

The function $N(\tau)$ has the property to pass over for small values of its argument to the argument itself. Therefore it is obvious to state for the whole range of α- and τ_N -values as a hypothesis the relation

$$N(\tau_{MAX}) = \alpha \cdot N(\tau_N). \tag{30}$$

This procedure of evaluation for the real occurring stress τ_{MAX} satisfies the following four conditions:

a) For small values of τ_{MAX} and τ_N the transition to Hooke's law is granted, for because of $N(\tau_{MAX}) \to \tau_{MAX} \to \tau_i$ and $N(\tau_N) \to \tau_N$ eq.(30) gives the definition equation of the elastic (Hookian) stress concentration factor $\tau_i = \alpha \cdot \tau_N$.

b) For small values of τ_N but arbitrary finite values of τ_i and τ_{MAX}, i.e. for great values of α , eq.(30) becomes $\tau_i(\tau_{MAX}) = \alpha \cdot \tau_N$ (because of $N(\tau_{MAX}) \to \tau_i(\tau_{MAX})$, $N(\tau_N) \to \tau_N$)as it must be.

c) For all stress-values $N(\tau_{MAX})$ and τ_i are always greater than the real stress τ_{MAX} in accordance with the physical behaviour of the materials.

d) For $\alpha = 1$ the notch-effect vanishes not only in the linear (Hookian) range but also for arbitrary $F(\tau)$. There is always $N(\tau_{MAX}) = N(\tau_N)$ and also $\tau_{MAX} = \tau_N$.

It can be seen that the hypothesis laid down in eq.(30) satisfies all of the conditions which can be thought of. Herewith a rather simple procedure is obtained for the determination of the real occurring stress from the ESCF and the nominal stress. The practical handling of the resulting nomographic method already has been illustrated in section 1 and by means of Fig.1.

It may be remarked that this relationship is also applicable as hypothesis for other deformation-laws without contradiction. Investigations in this direction and the checking of the outlined theory by means of experimental data are presently being made.

II. EXPERIMENTAL PART

1. Static Tests

1.1. Materials used, Shapes of Specimens and Type of Tests

Tension- and bending tests with double-notched specimens and tension tests with bars having a shoulder fillet had been performed. The specimen shapes used are listed in Fig.5. All the specimens A were made from the Aluminum-alloy "Velodur", the specimens C from Steel St.00.21 and the filleted bars B from "Velodur" as well as from Steel St.00.12. The stress-strain curves of the materials can be seen in Fig.6, the according values of tensile strength, Young's modulus and shear modulus are listed below (dimension kg/mm^2)

	St.00.12	St.00.21	Velodur
Tensile strength	32,6 - 39,3	45,9 - 46,1	52,7 - 57,8
Young's modulus	$2{,}147.10^4$	$2{,}072.10^4$	$0{,}720.10^4$
Shear modulus	$0{,}806.10^4$	$0{,}817.10^4$	$0{,}273.10^4$

The specimens A and B were used for tension tests, the specimens C for bending tests. In the tension- and bending tests with the specimens A and C the strains were measured by electrical strain-gages, whereas the tension-tests with specimens B were performed by means of the photoelastic stress-coat method. The thickness of the cemented Araldite layers was 2 mm for the Velodur specimens and 4 mm for the steel specimens. A casting equipment had been built by means of which Araldite plates with exactly constant thickness could be fabricated.

Electrical strain gages which were mounted in the notch served as control.
We performed each test two times i.e. with two identical specimens.

In the tension test a new clamping equipment with spherical joint bearing (cf.Fig.7), which was manufactured by us, came into operation. This clamping method granted a tensile loading of the specimen which was largely free of bending.
The equipment used for the bending tests is shown schematically in Fig.8. Besides this the experimental work was done by means of the same machines and measuring instruments as in former tests (see [1]). Also the performance of the tests and the analysis of the measuring results were made as described in [1] so that there is no need to go into further details of it.

1.2 Results of the Tests

The results of the tension tests with the double-notched specimens according Fig.5,A (material "Velodur") are laid down in Figs. 9 to 16. Fig.9 shows the dependence of the ESCF α on the notch angle.(In this diagram ▲ means the extreme values measured, o the mean values). As can be seen the flank angle exerts a considerable influence on the ESCF only for $\omega > 90^{\circ}$. Therefore the curves of the stress distribution over the minimum section in the elastic range practically coincide for $\omega = 0^{\circ}$, 45° and 90°, see Fig.10. The stress distribution for $\omega = 135^{\circ}$ is represented in Fig.11. In the plastic range the stress concentration factor (SCF) σ_{MAX}/σ_N depends on the nominal stress σ_N as well as on the material; σ_{MAX}/σ_N vs. σ_N is plotted in Fig.12. Figures 13 and 14 show the distribution of strains over the minimum section measured for various nominal stresses for $\omega = 0^{\circ}$, 45°, 90° and $\omega = 135^{\circ}$ respectively. From Fig.15 the distribution of the remaining strains over the minimum section after unloading can be seen for specimens with notch angle $\omega = 0^{\circ}$, 45°, 90°. The largest nominal stress before the unloading was $\sigma_N = 24{,}1$ kg/mm^2

for the curves A and σ_N = 28,2 kg/mm^2 for the curves B. For the notch-angle $\omega = 135^\circ$ Fig.16 is analogously valid. Herewith corresponds σ_N = 20,0 kg/mm^2 to the curves A and σ_N = 28,2 kg/mm^2 to the curves B.

The results for the double-notched bending specimens according Fig.5,C (material Steel St.00.21) are shown in Figs. 17 to 30. The dependence of the ESCF α on the notch angle is plotted in Fig.17 (▲ extreme values, o mean values) whereas the stress distributions in the elastic range can be seen in Figs. 18 to 21. For the dependence σ_{MAX}/σ_N on σ_N the curves in Fig.22 were obtained.
The strain distributions over the minimum section in the plastic range for the notch angles $\omega = 0^\circ$, 45°, 90°, 135° are shown in the Figs. 23, 24, 25, 26 respectively.

The remaining strains after unloading for the specimens with $\omega = 0^\circ$, 45°, 90° and 135° are represented in Figs. 27 to 30. Herewith the curves B correspond to a largest nominal stress σ_N = 31,5 kg/mm^2 before unloading and the curves A to σ_N = 35,0 kg/mm^2. As the strains measured in the plastic range proved to be practically the same in magnitude on the tension side of the bar as well as on the pressure side, in the Figs. 23 to 30 only the strains for the tension region are plotted.

The tension tests with filleted bars according Fig.5,B (material "Velodur" and Steel St.00.12) by means of the photoelastic stress-coat method (cf. Fig.31 as an example of an isochromatic pattern for a Velodur specimen with $a/\varrho = 4$ at σ_N = 45 kg/mm^2) furnished the dependence of the SCF σ_{MAX}/σ_N on σ_N as laid down in Fig.32. Figs. 33 and 34 show the stress distribution along the edge for the Velodur specimens with $a/\varrho = 2$ and $a/\varrho = 4$ for various nominal stresses (plastic range). In Fig.35 the distribution of the remaining strains along the edge after unloading is plotted for a Velodur specimen with $a/\varrho = 2$. The curves b and a herein correspond

to a largest nominal stress before unloading σ_N = 38,8 kg/mm^2 and σ_N = 47,75 kg/mm^2 respectively. Analogously Fig.36 stands for a/ϱ = 4, the curves c, b and a concerning σ_N = 35,25 kg/mm^2, 39,25 kg/mm^2 and 41 kg/mm^2 respectively. The indices 1 and 2 in Figs. 35 and 36 mean the results of different specimens.

The Velodur specimens proved to be very suitable for the photoelastic stress coat tests, whereas the isochromatic patterns of the steel specimens were unsatisfactory. Therefore in the case of the latter no stress distributions along the edge could be determined.

2. Fatigue tests

Push-pull fatigue tests had been carried out with specimens according to Fig.37. One Wöhler curve had been performed for the unnotched specimens and for the specimens with a central hole (ratio a/ϱ = 3 and a/ϱ = 4) at a stress ratio

$$K = \frac{\text{minimum stress}}{\text{maximum stress}} = 0.$$

The specimens had been machined from a 200 mm x 5 mm rolled bar of the material St.00.12. The rolling skin was not worked off. The testing machine used is a Schenck 20 t push-pull machine, type PPD 20, with a cycle frequency of 2200 cycles per minute.

Figs. 38, 39 and 40 show the test results for the specimen shapes investigated.

III. BIBLIOGRAPHY

[1] Research on the Distribution of Tension in Notched Construction Parts. By H. Neuber Contract AF 61(514)-1111, WADD Technical Report. 60-906

[2] H. Neuber: Kerbspannungslehre Second Edition, Berlin 1958

IV. ILLUSTRATIONS

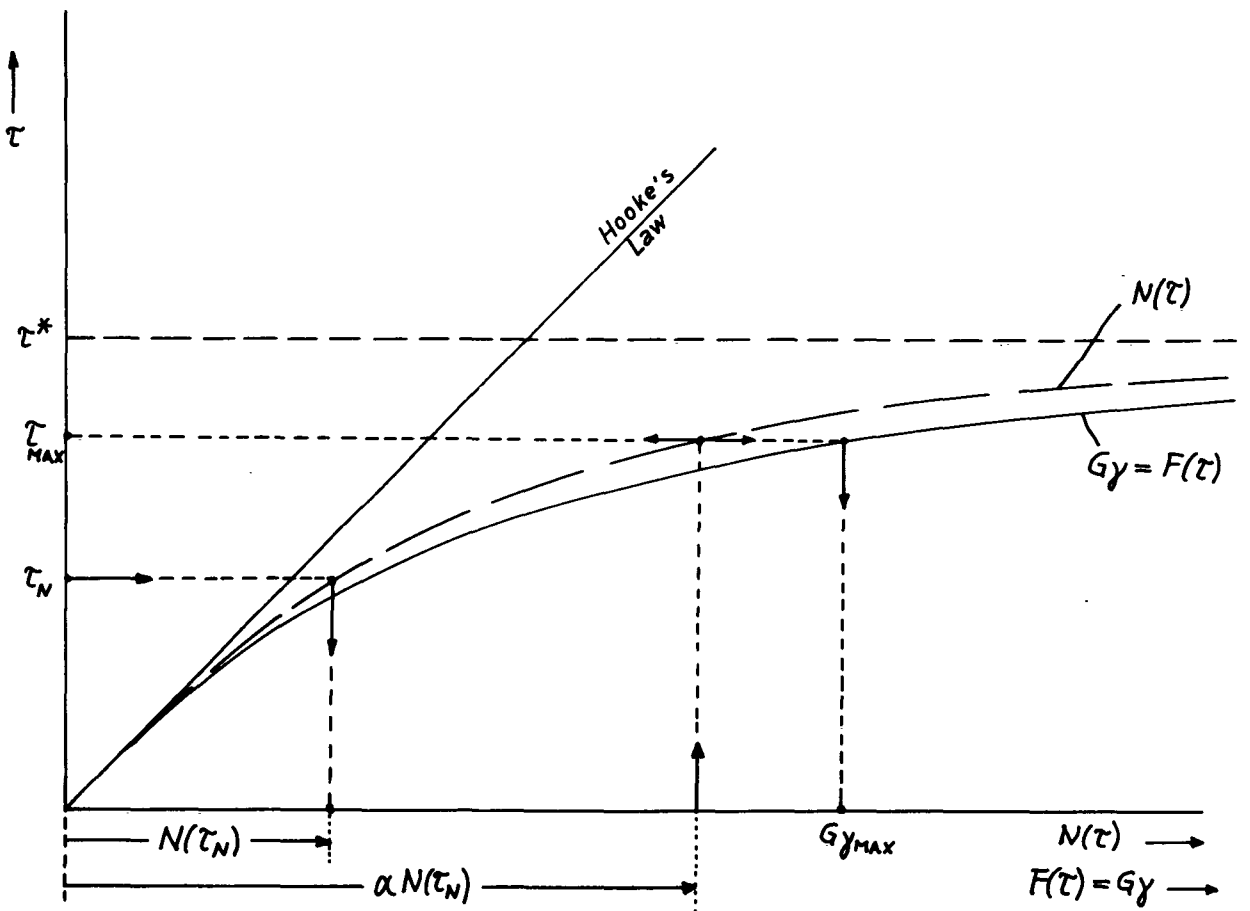

Fig. 1 Nomographic method for determination of stress- and strain concentrations for shear

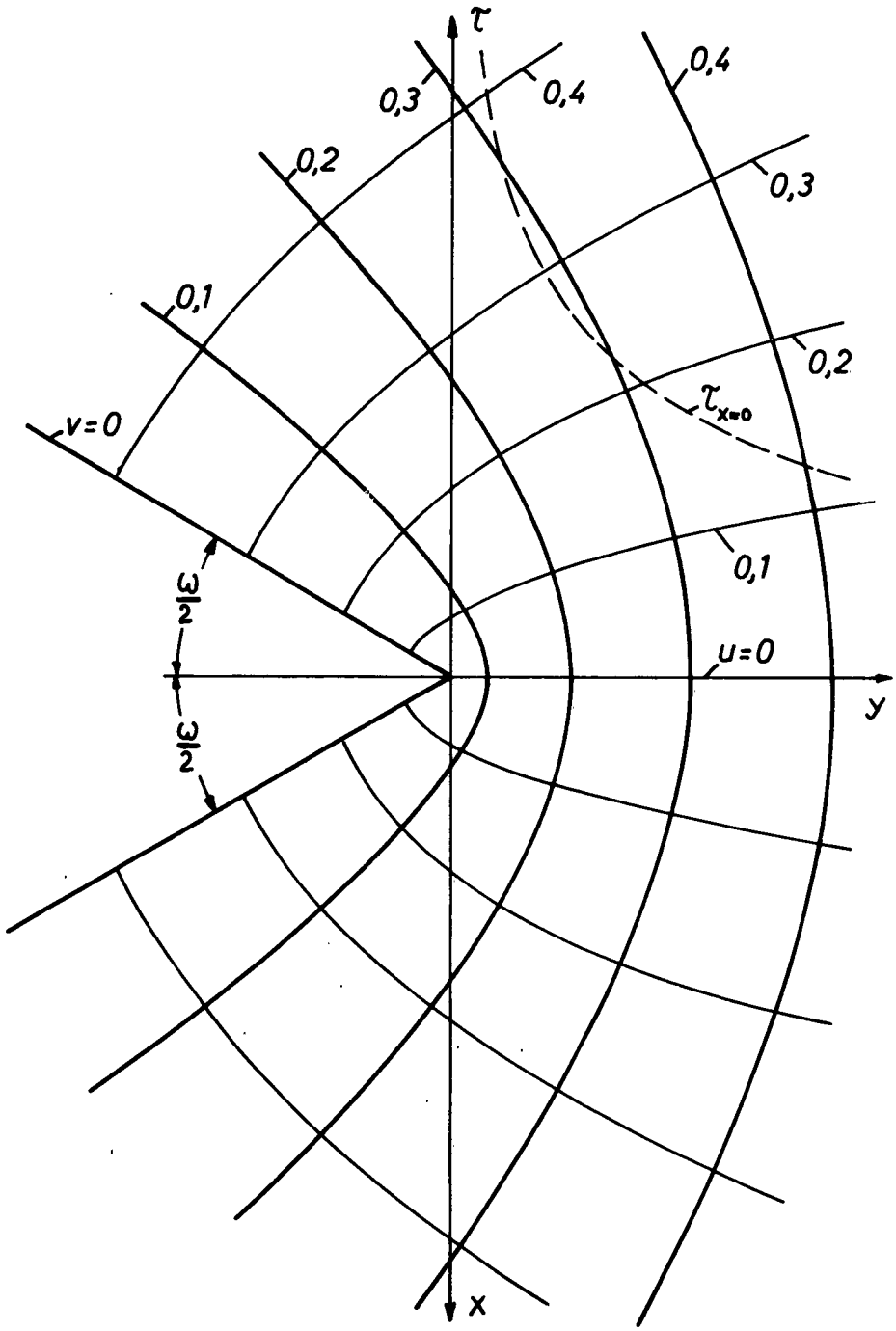

Fig.2 Stress- and warping lines for a 60°-notch (Hookian range) and stress distribution along x = 0

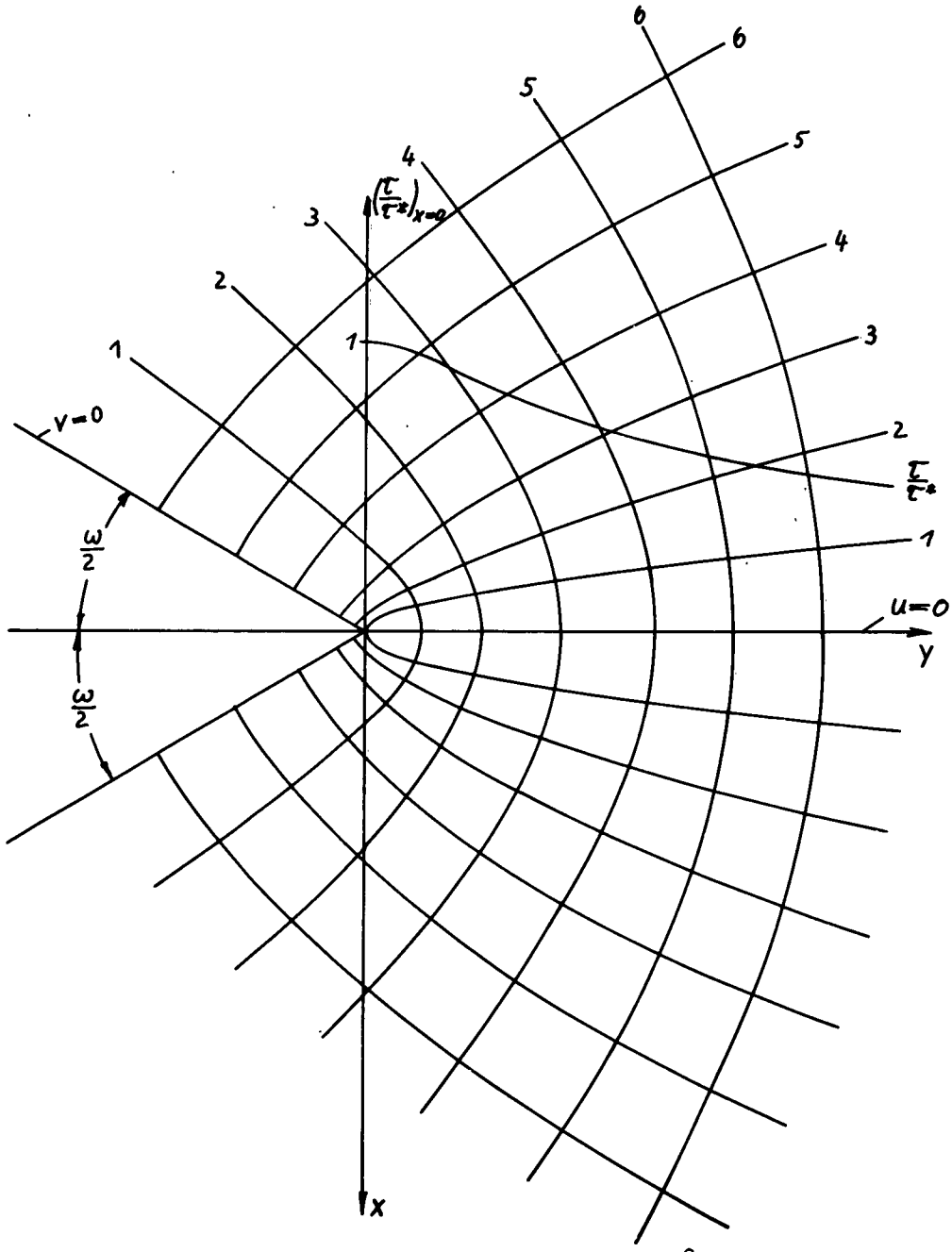

Fig. 3 Stress- and warping lines for a 60°-notch (non-linear law (1)) and stress distribution along x = 0

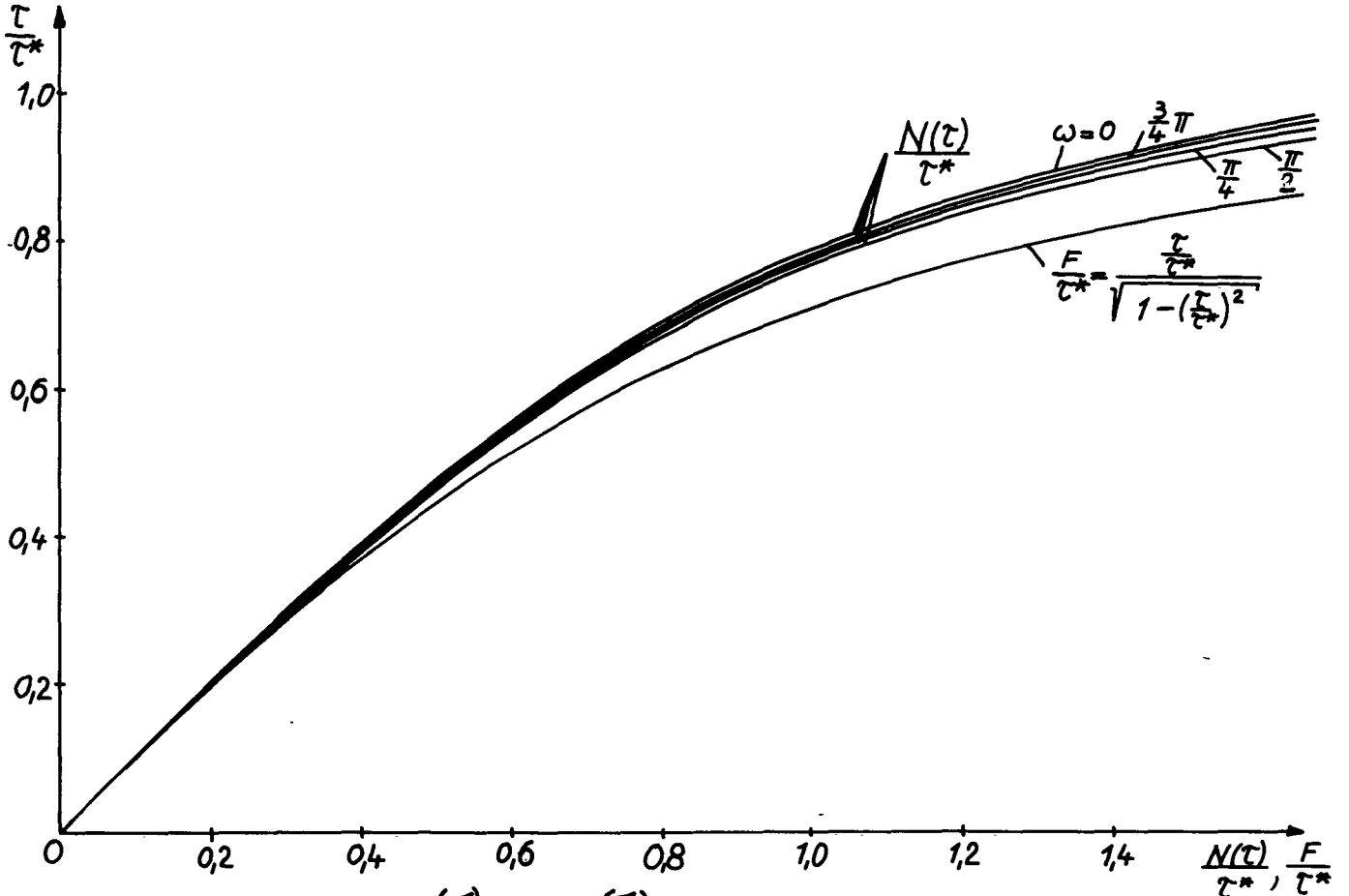

Fig.4 The functions $N(\tau)$ and $F(\tau)$

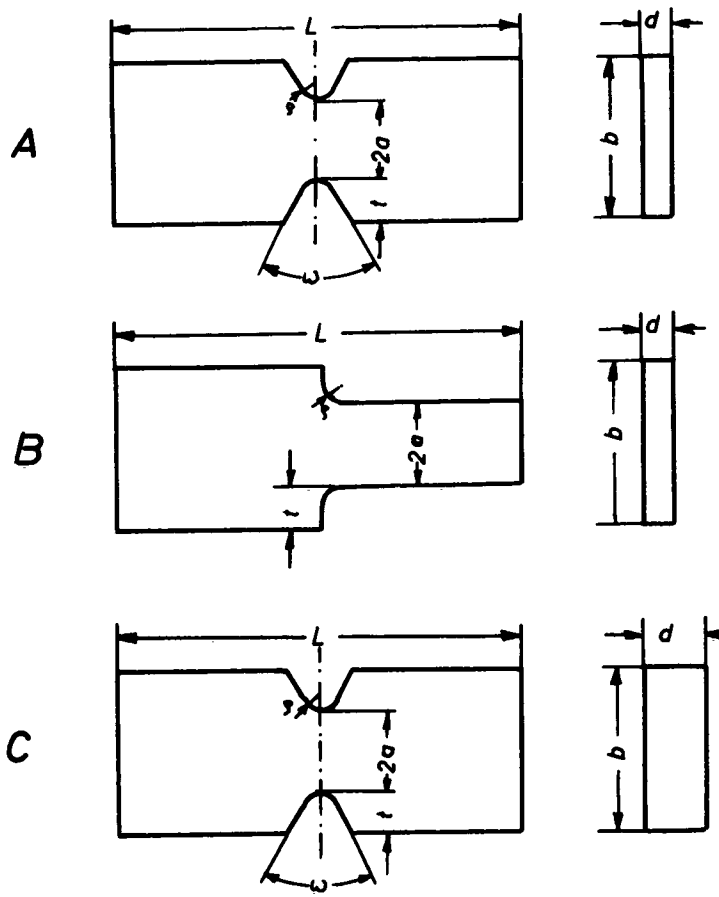

ω°	a/ϱ	ϱ	a	t	d	b	L
0	4	12,5	50	50	5	200	800
45							
90							
135							

a/ϱ	ϱ	a	t	d	b	L
2	25	50	50	5	200	800
4	12,5					

ω°	a/ϱ	ϱ	a	t	d	b	L
0	4	12,5	50	50	30	200	1500
45							
90							
135							

Fig.5 Shapes and dimensions of the specimens used

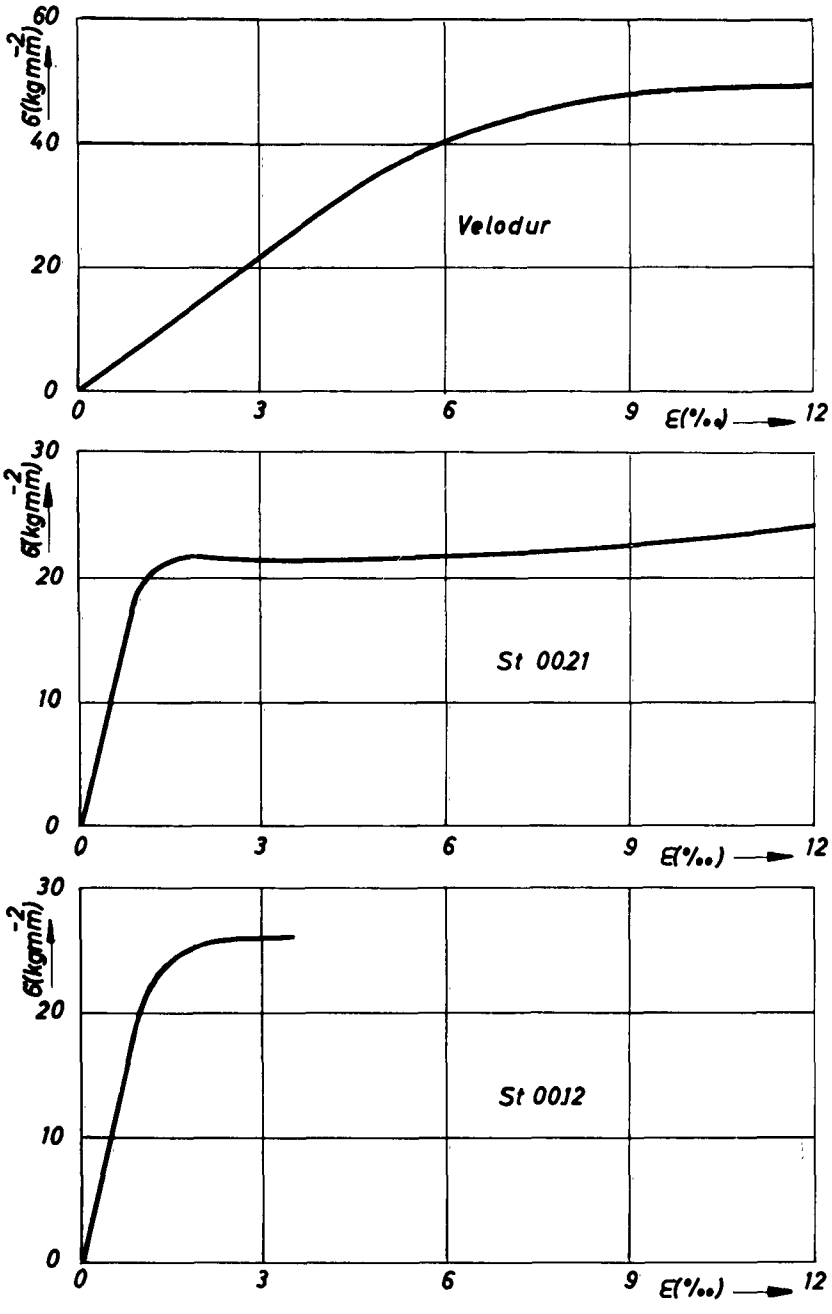

Fig.6 Stress-strain curves for the materials used

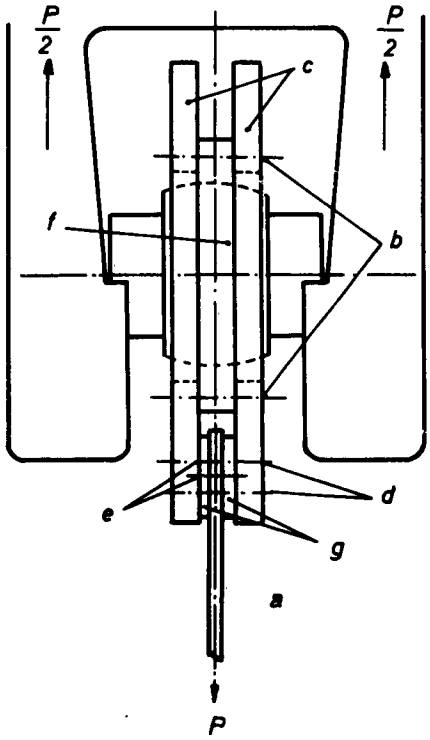

a tension bar
b screws for bearing attachment
c cover plates
d screws for clamping
e fitting pins
f spherical joint bearing
g roughened intermediate plates

Fig.7 Clamping device with spherical joint

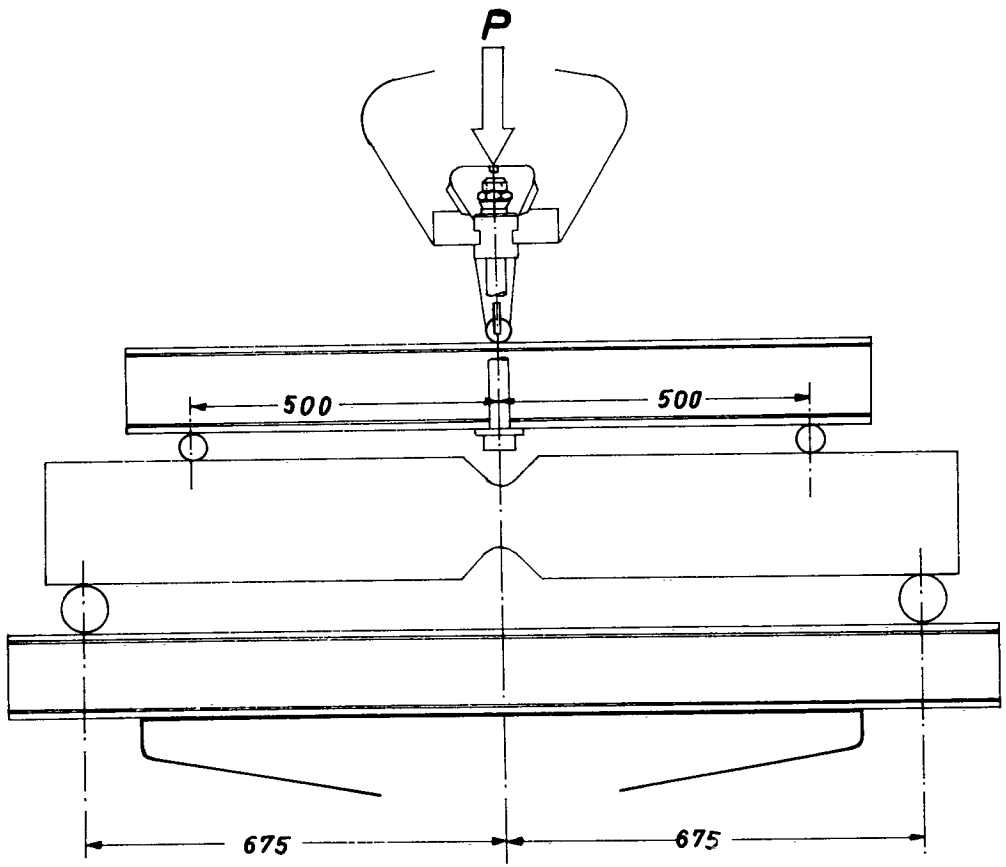

Fig. 8 Loading-equipment for bending tests

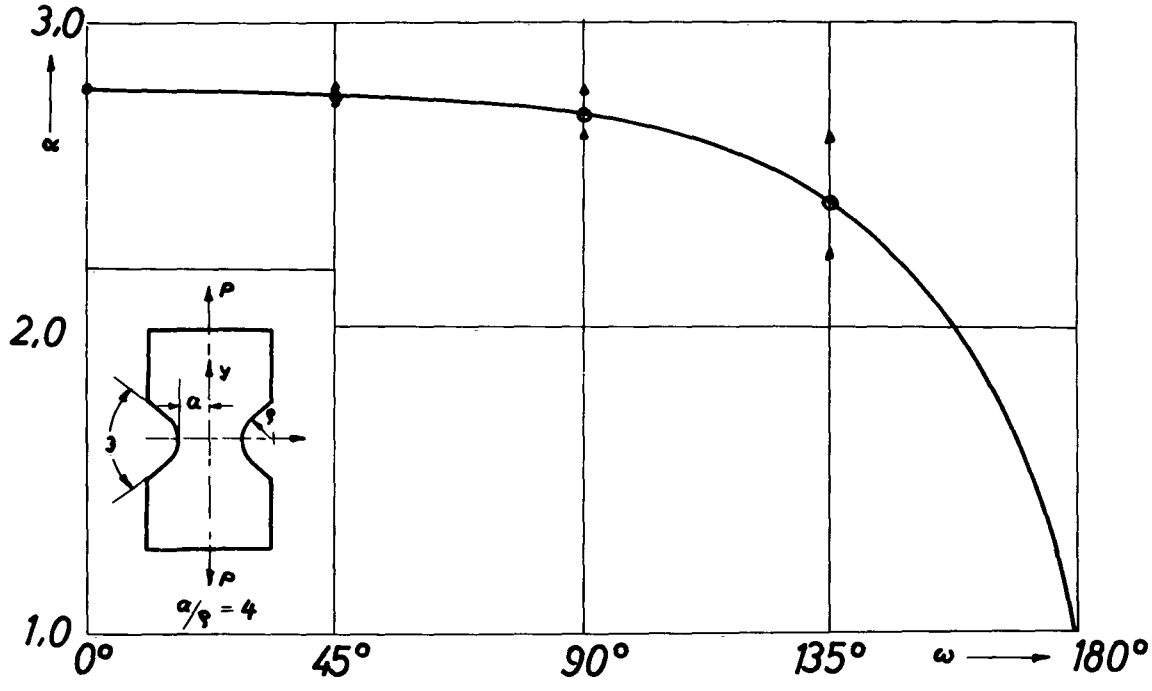

Fig. 9 ESCF α vs. notch angle ω for a double notched tension bar

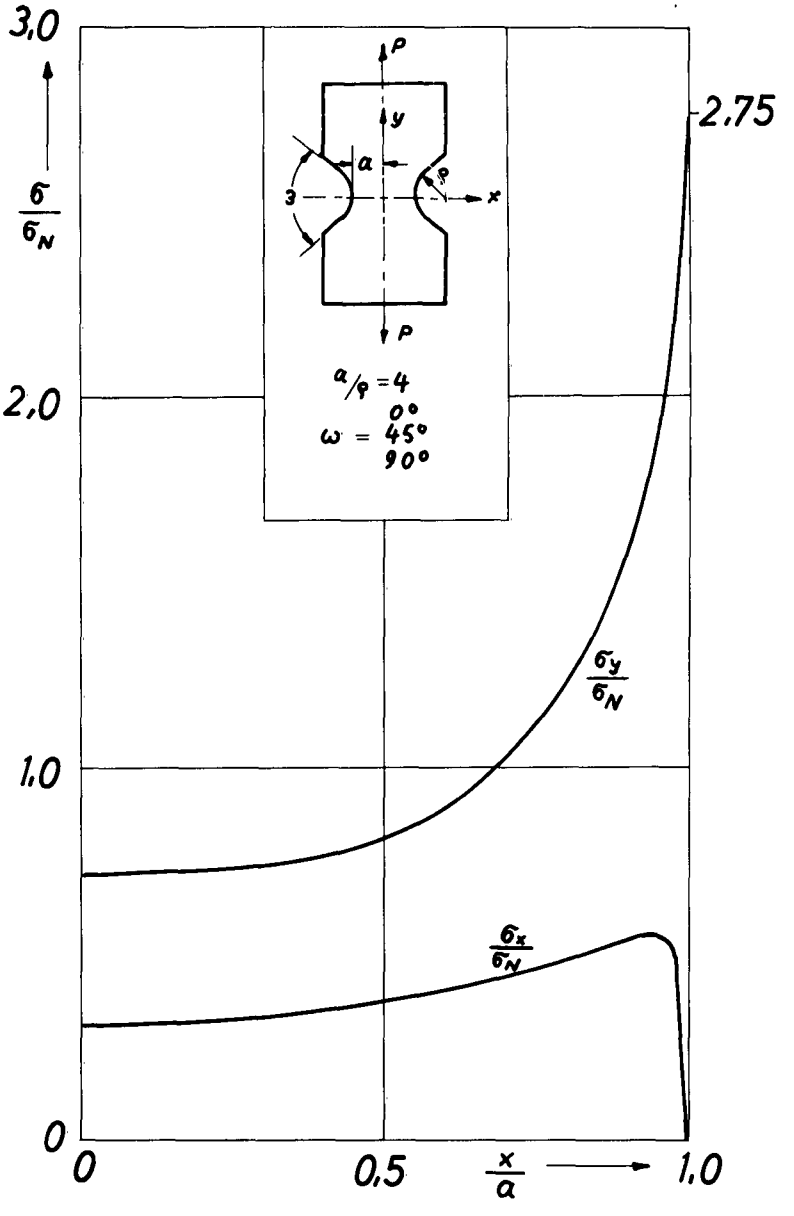

Fig.10 Stress distribution over the minimum section of a double notched tension bar for $\omega = 0^{\circ}, 45^{\circ}, 90^{\circ}$; $a/\rho = 4$ (elastic range)

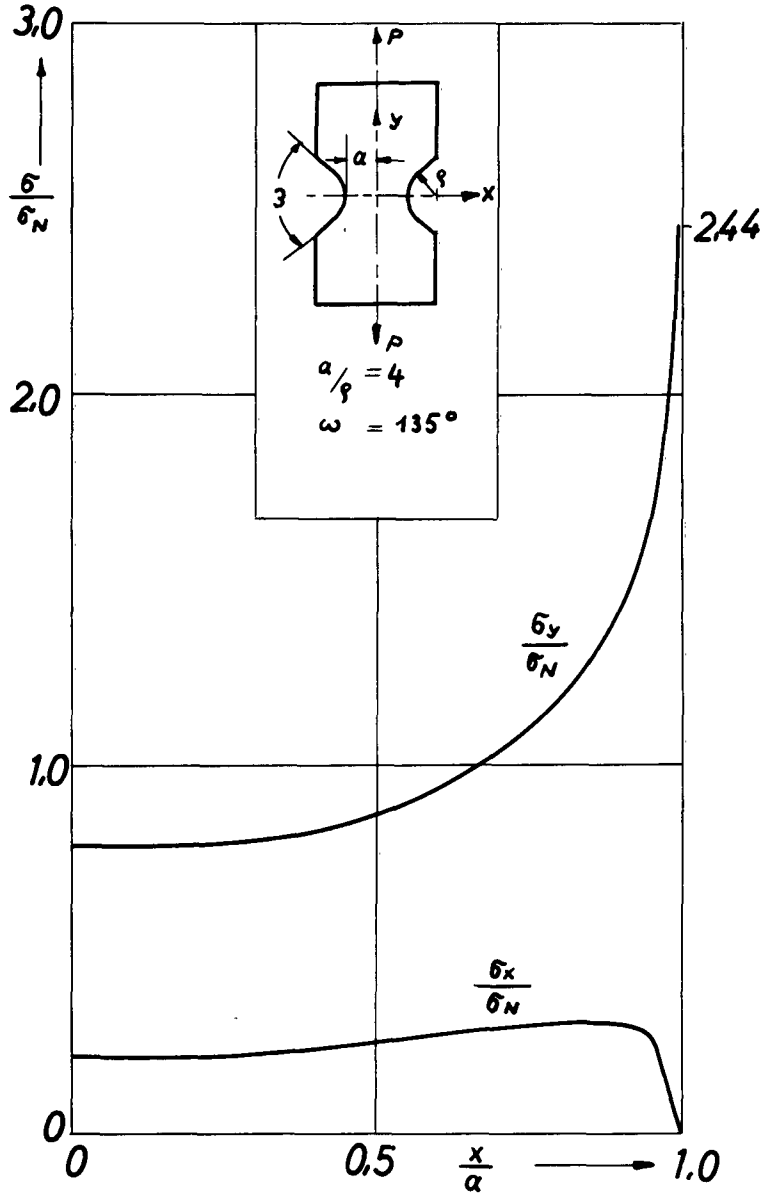

Fig.11 Stress distribution over the minimum section of a double notched tension bar for $\omega = 135^{\circ}$; $a/\rho = 4$ (elastic range)

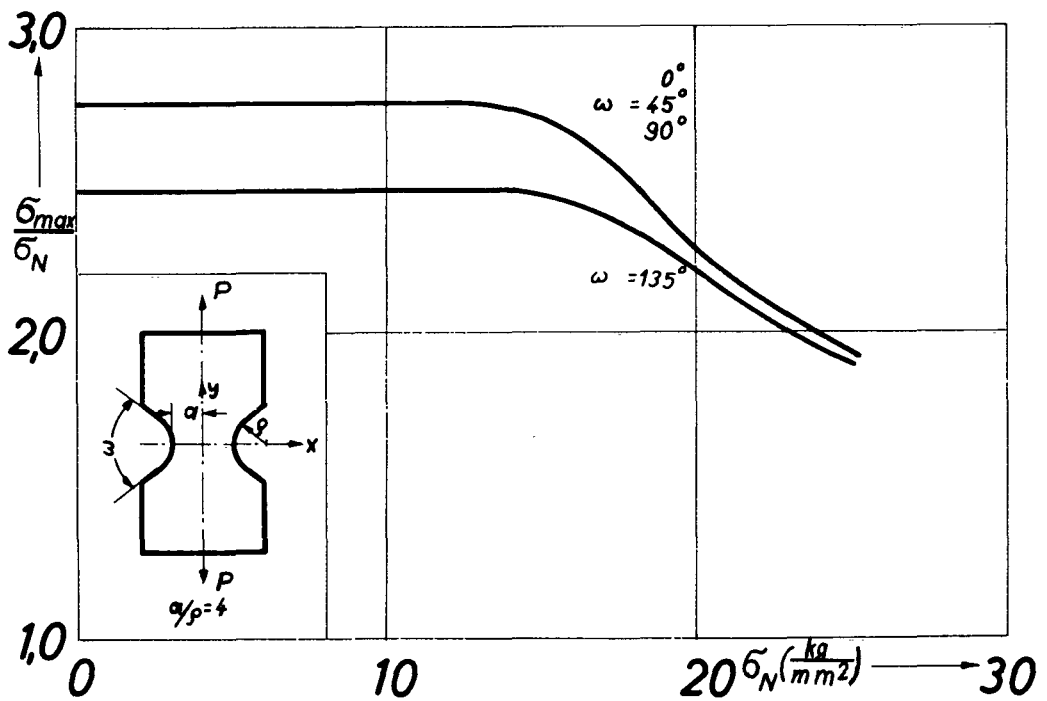

Fig.12 SCF σ_{MAX}/σ_N vs. σ_N for a double-notched tension bar, $a/\rho = 4$, $\omega = 0^\circ$, 45°, 90° and $\omega = 135^\circ$ (Material: "Velodur")

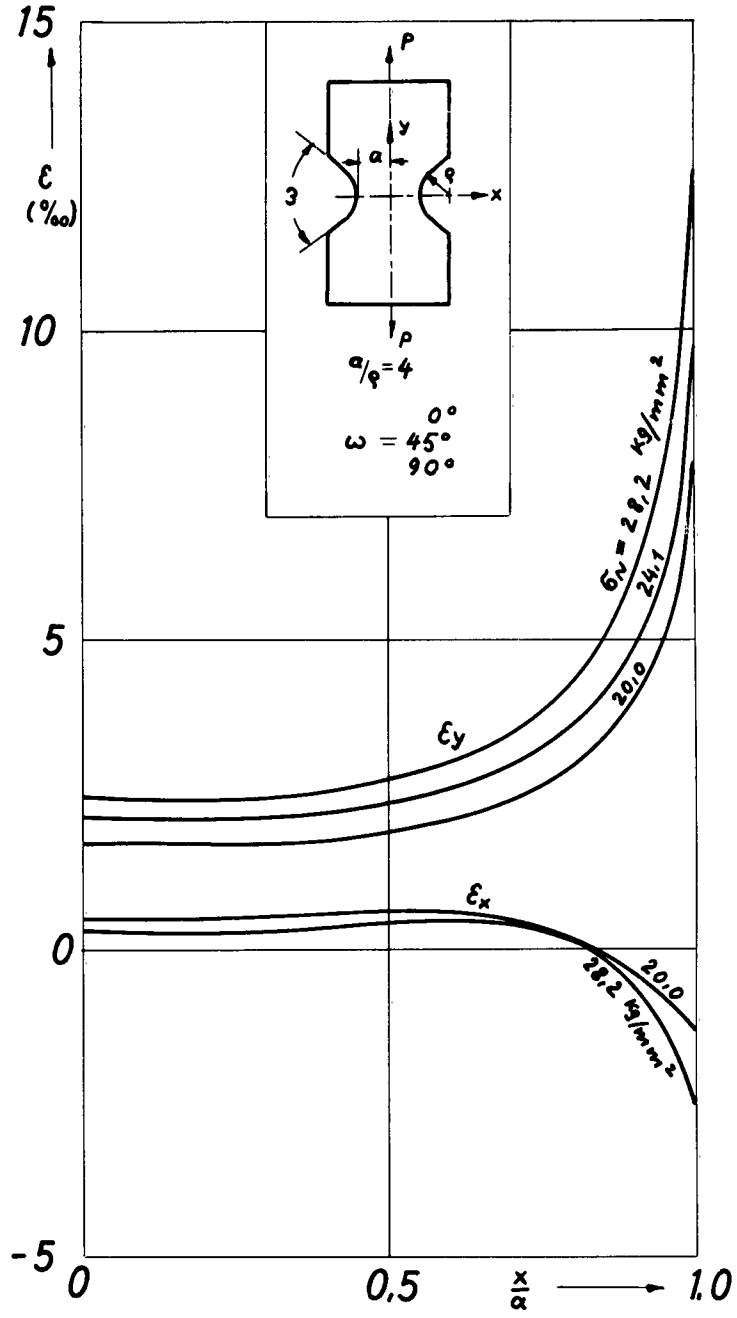

Fig.13 Strain-distribution over the minimum section of a double-notched tension bar, $a/\rho = 4$, $\omega = 0^0, 45^0, 90^0$ for various σ_N (Material "Velodur", plastic range)

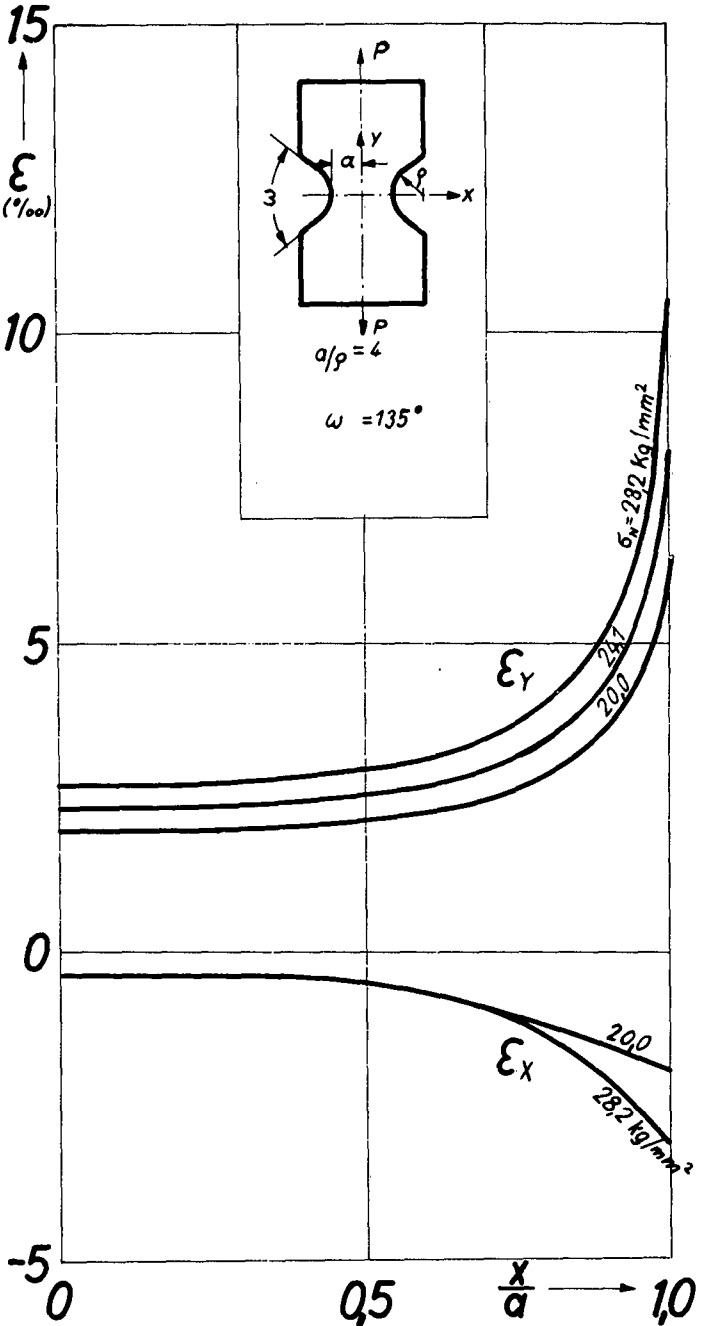

Fig.14 Strain-distribution over the minimum section of a double-notched tension bar, $a/\varrho = 4$, $\omega = 135^{0}$ for various σ_N (Material "Velodur", plastic range)

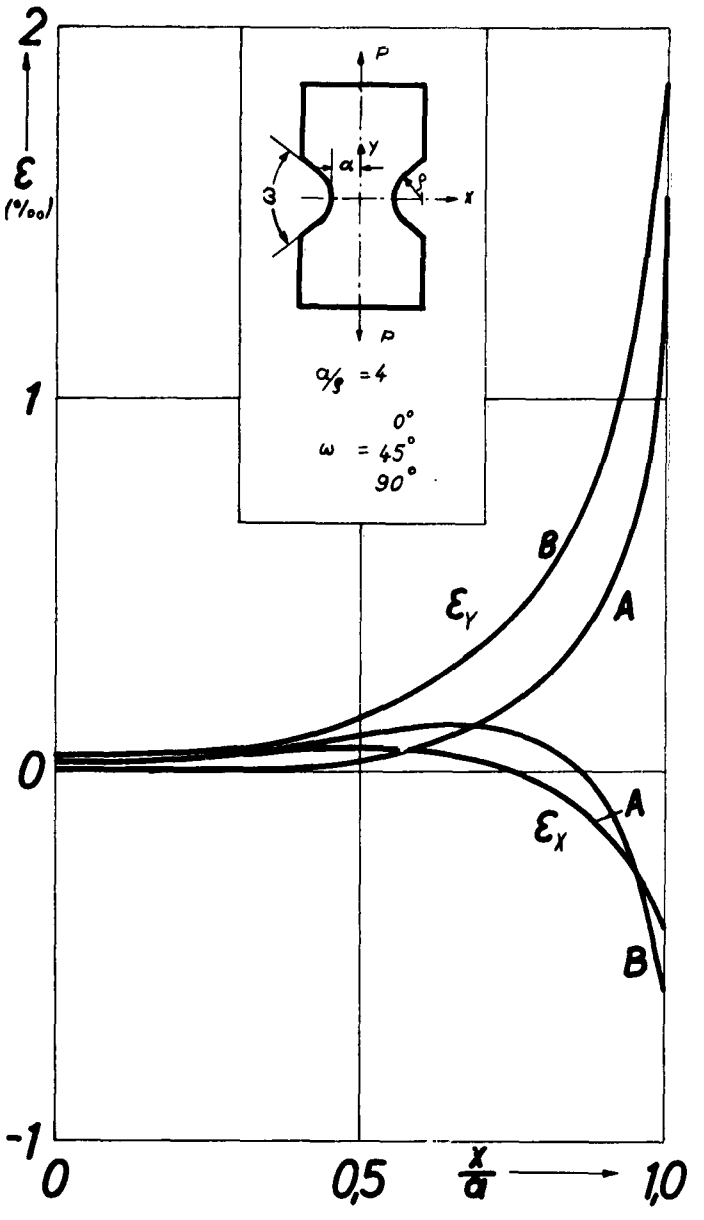

Fig.15 Distribution of the remaining strains over the minimum section of a double-notched tension bar ($a/\rho = 4$, $\omega = 0^{\circ}, 45^{\circ}, 90^{\circ}$; material "Velodur")

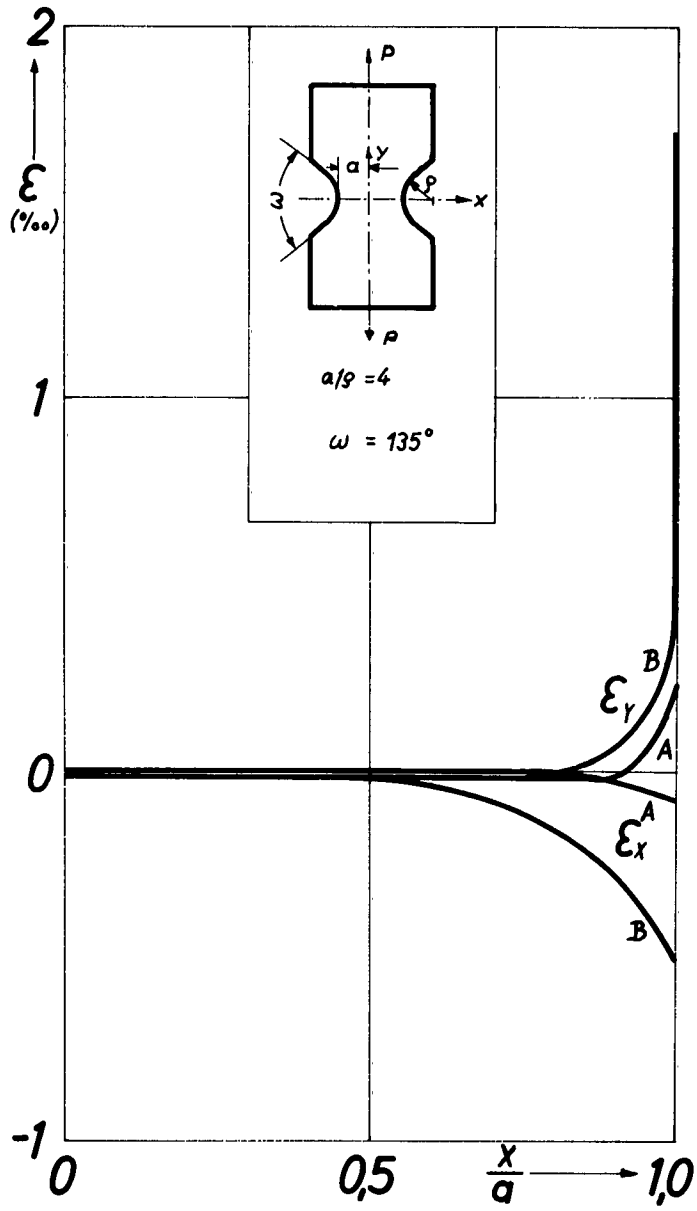

Fig.16 Distribution of the remaining strains over the minimum section of a double-notched tension bar ($a/\rho = 4$, $\omega = 135^{\circ}$; material "Velodur")

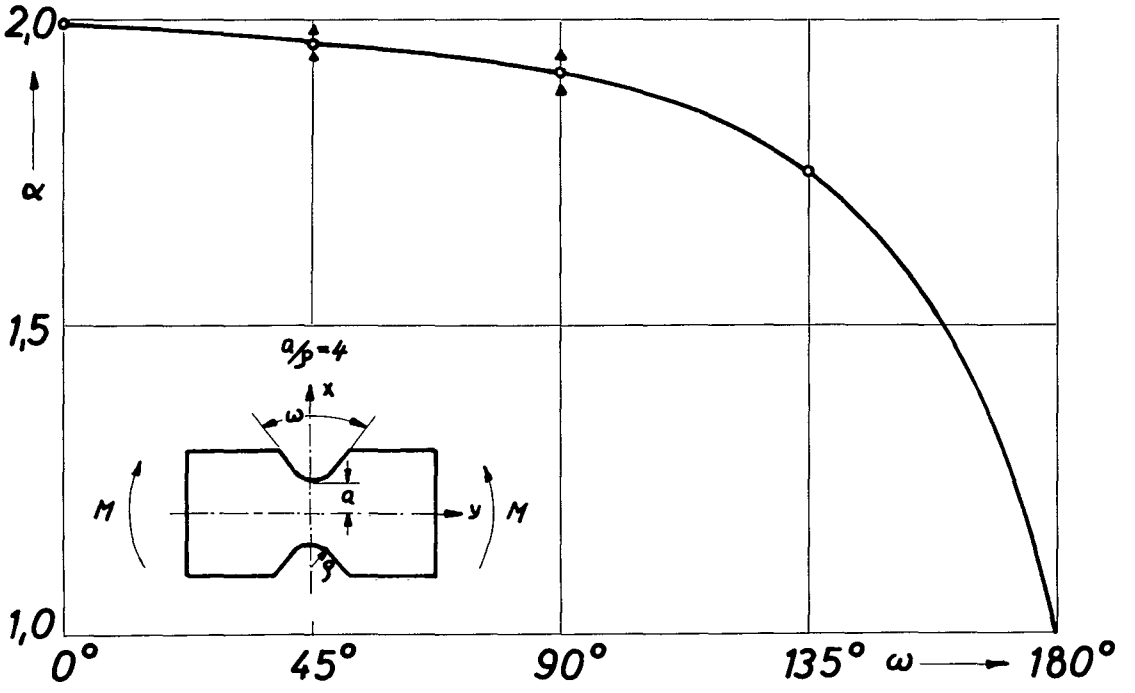

Fig.17 ESCF α vs. notch-angle ω for a double-notched bending bar

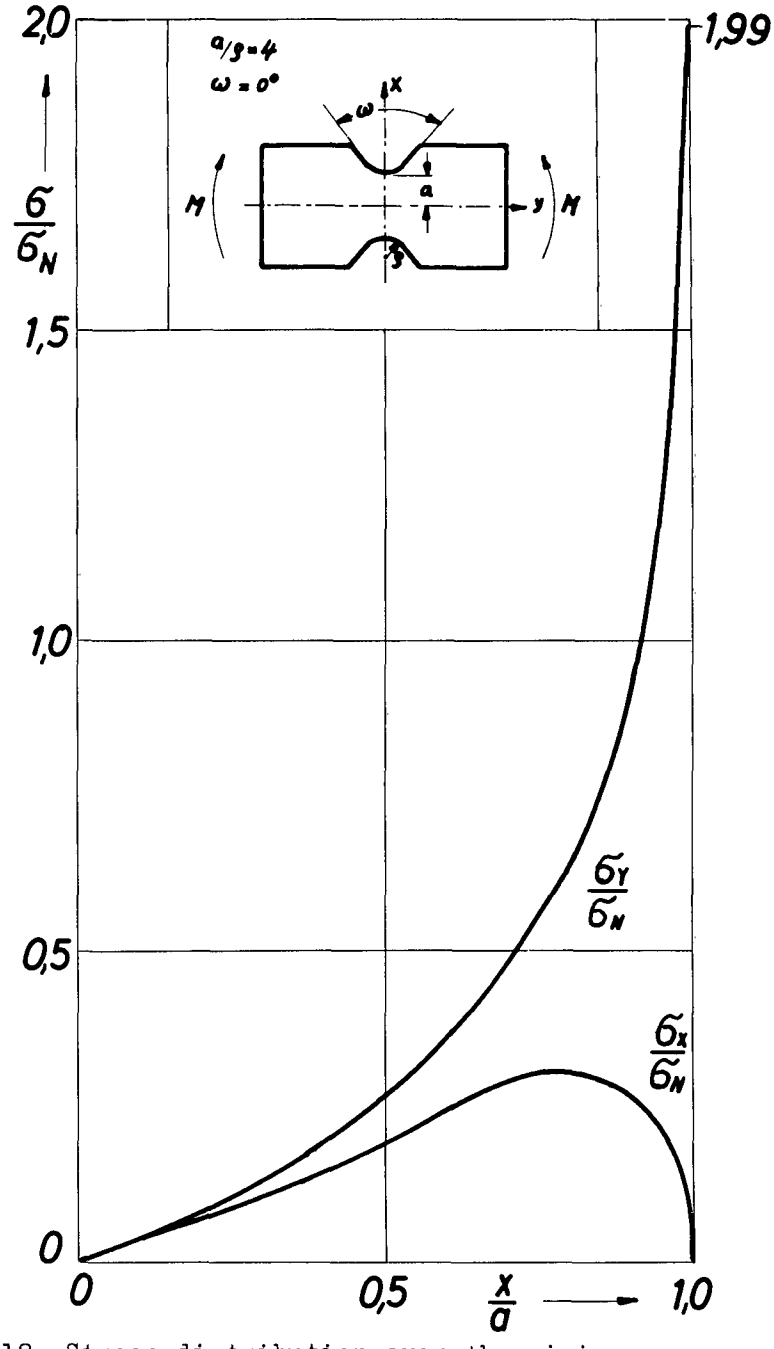

Fig.18 Stress-distribution over the minimum section of a double-notched bending bar with $a/\varrho = 4$, $\omega = 0^0$ (elastic range)

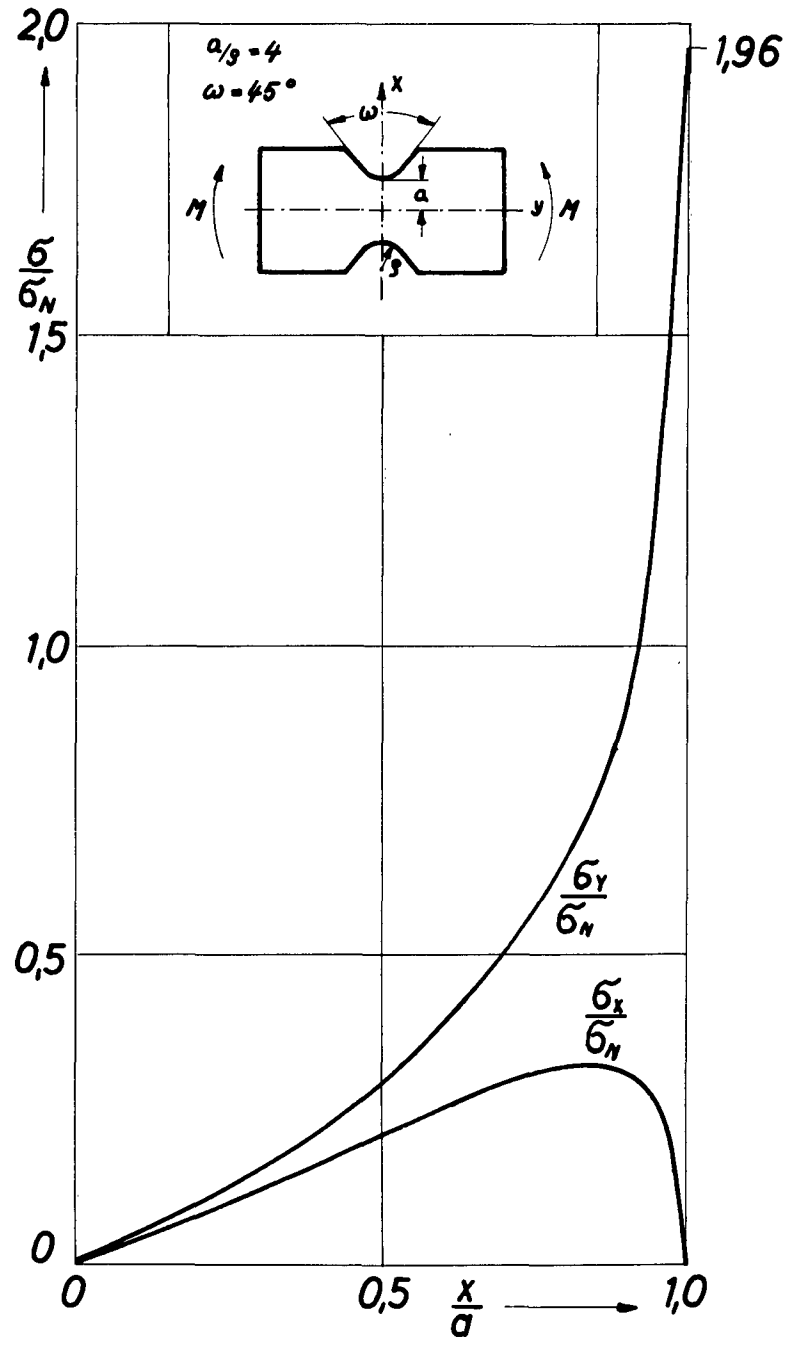

Fig.19 Stress-distribution over the minimum section of a double-notched bending bar with $a/\rho = 4$, $\omega = 45^{\circ}$ (elastic range)

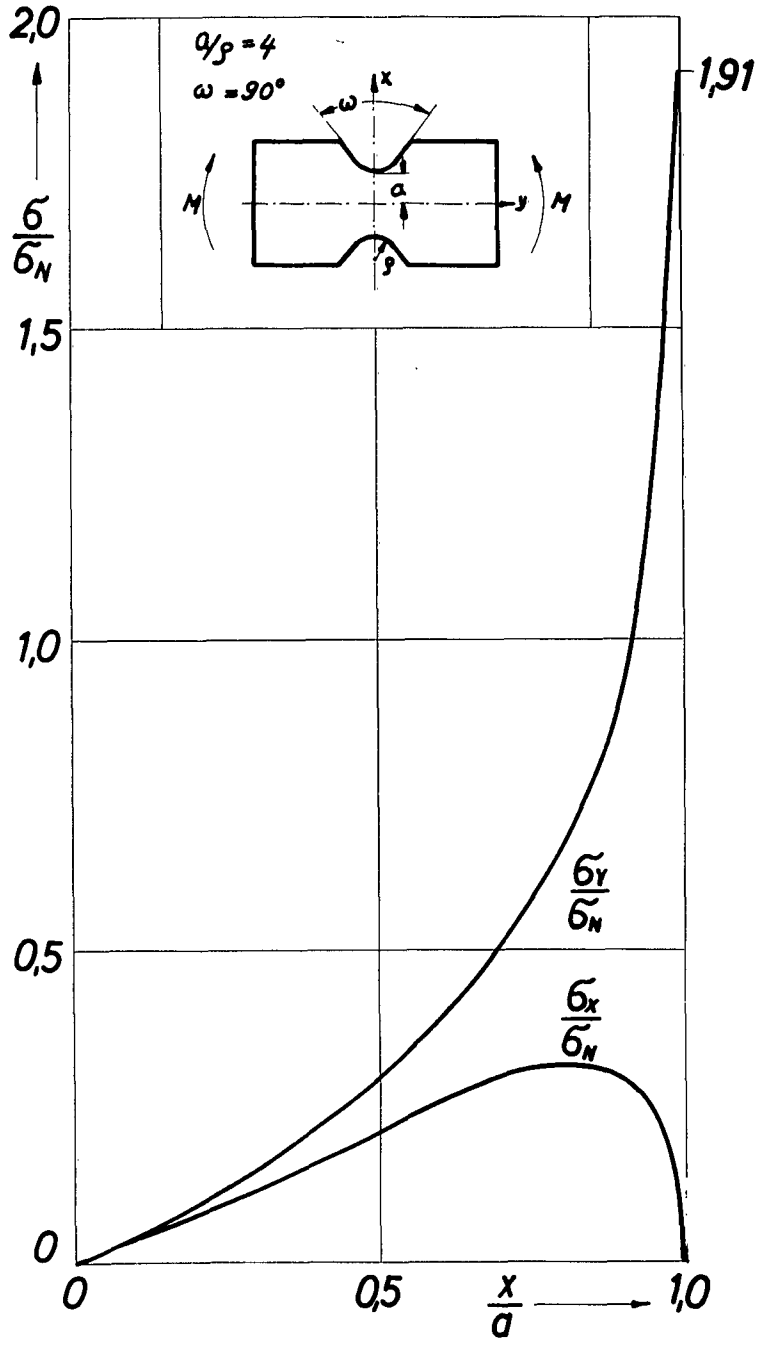

Fig.20 Stress-distribution over the minimum section of a double-notched bending bar with $a/\rho = 4$, $\omega = 90^{\circ}$ (elastic range)

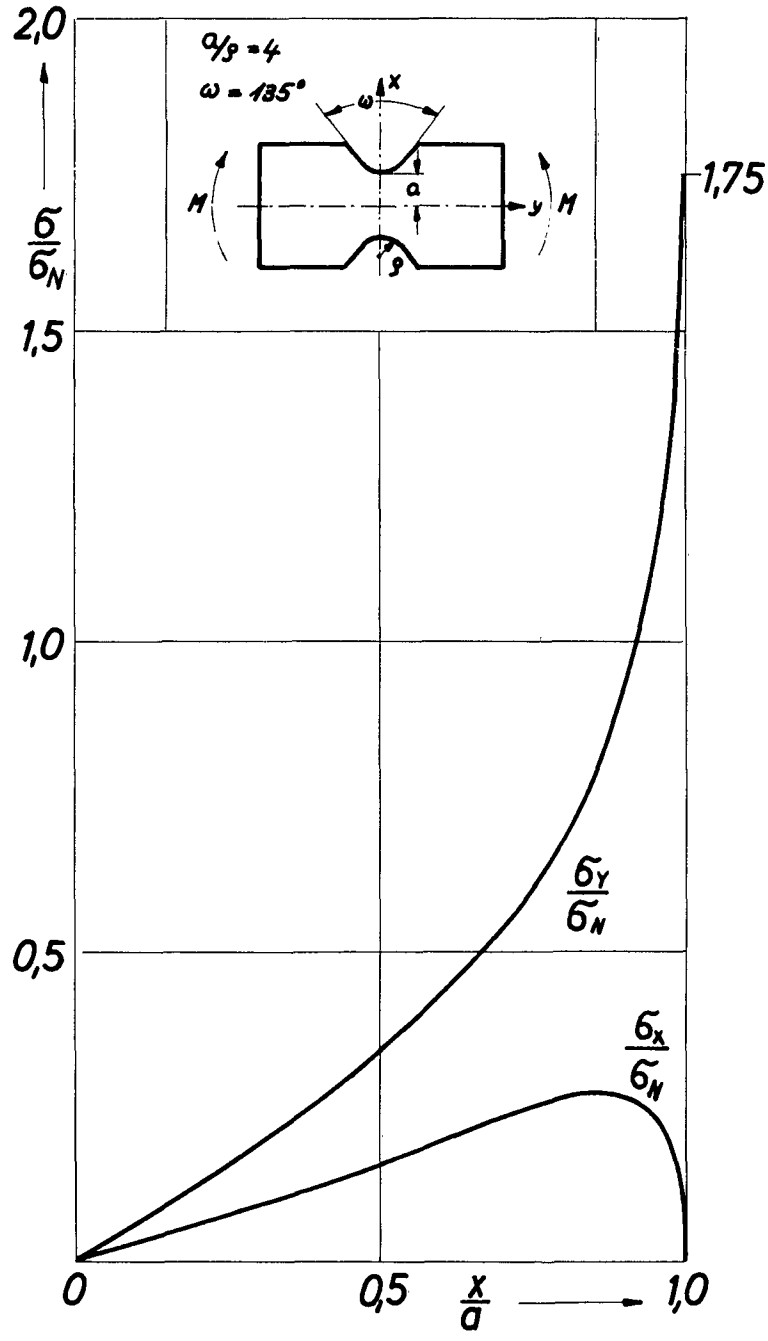

Fig.21 Stress-distribution over the minimum section of a double-notched bending bar with $a/\varrho = 4$, $\omega = 135^{\circ}$ (elastic range)

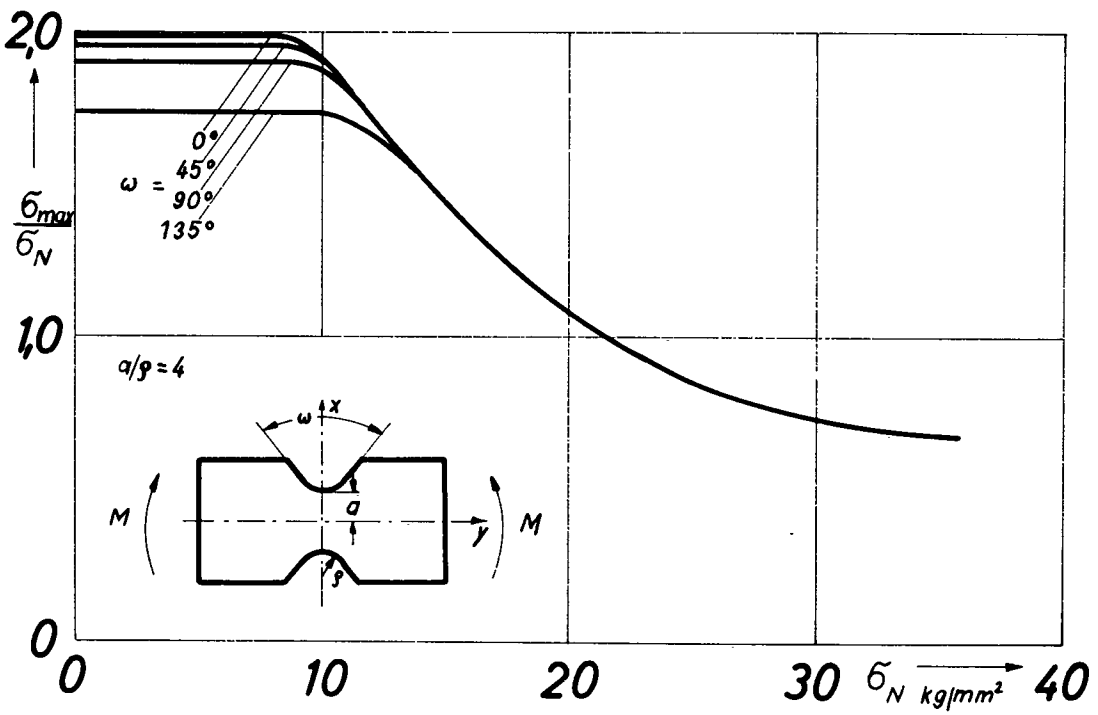

Fig.22 SCF σ_{MAX}/σ_N vs. σ_N for a double-notched tension bar, $a/\rho = 4$, $\omega = 0^\circ, 45^\circ, 90^\circ, 135^\circ$ (Material Steel St.00.21)

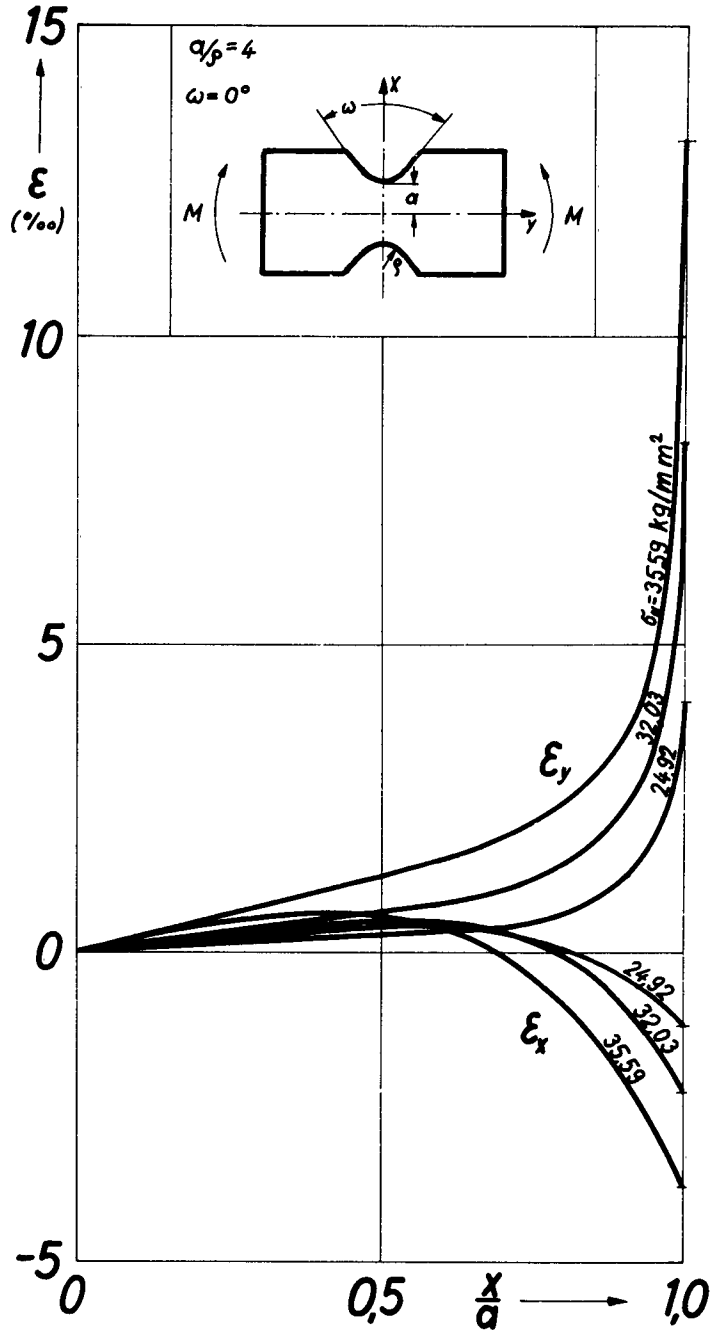

Fig.23 Strain-distribution over the minimum section of a double-notched bending-bar, a/ρ = 4, ω = 0° for various σ_N (Material Steel St.00.21, plastic range)

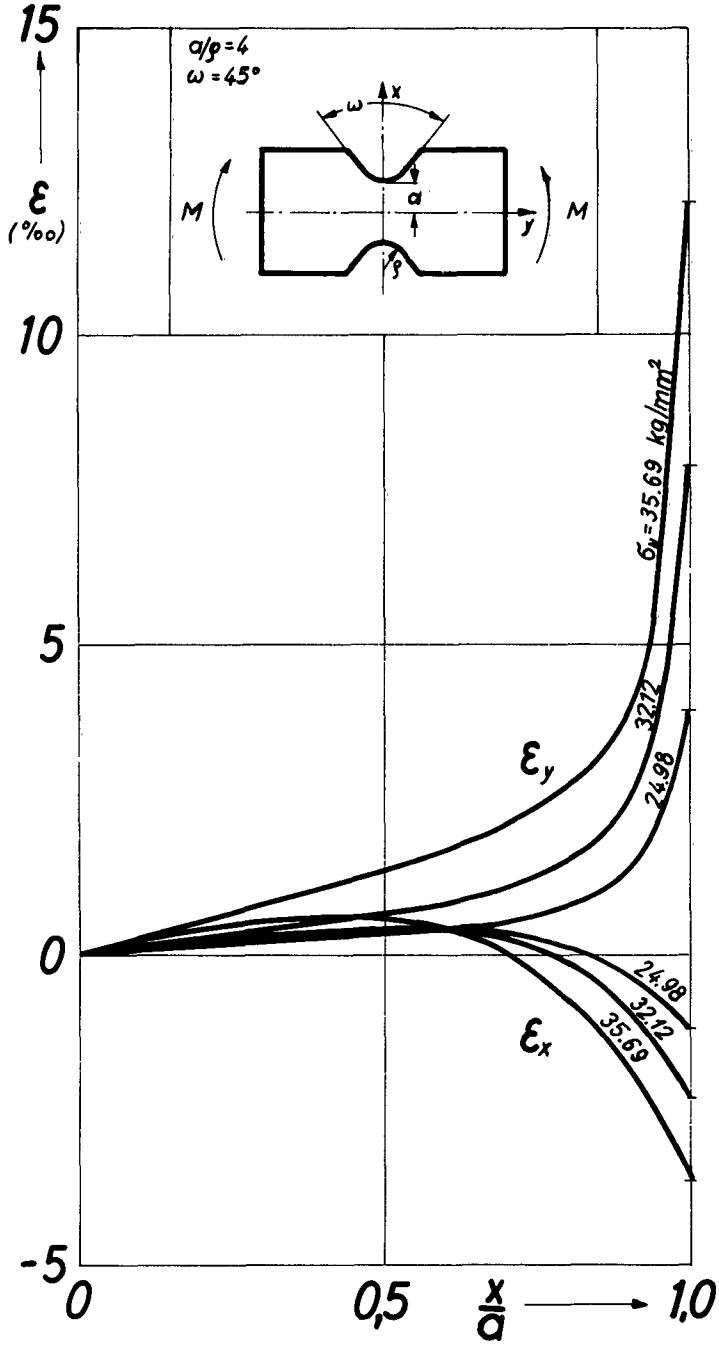

Fig.24 Strain-distribution over the minimum section of a double-notched bending-bar, $a/\rho = 4$, $\omega = 45°$ for various σ_v (Material Steel St.00.21, plastic range)

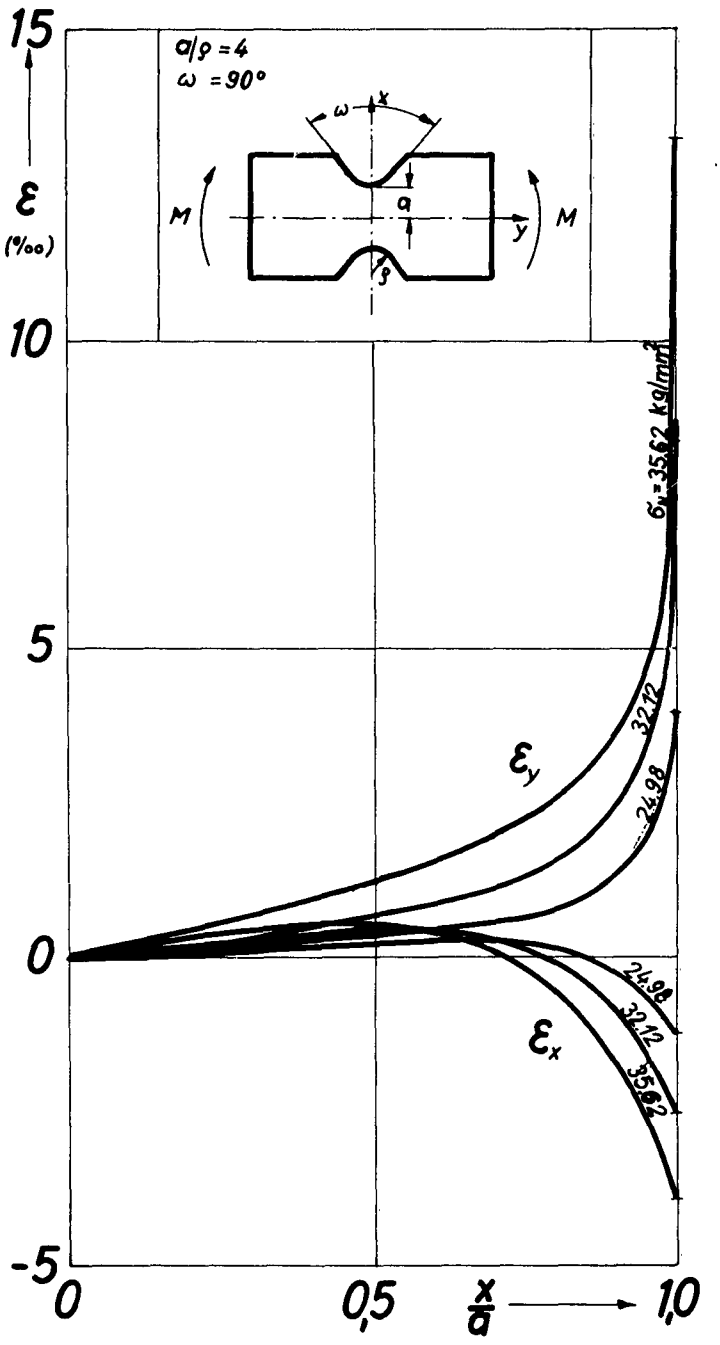

Fig.25 Strain-distribution over the minimum section of a double-notched bending-bar, $a/\rho = 4$, $\omega = 90°$ for various σ_N (Material Steel St.00.21, plastic range)

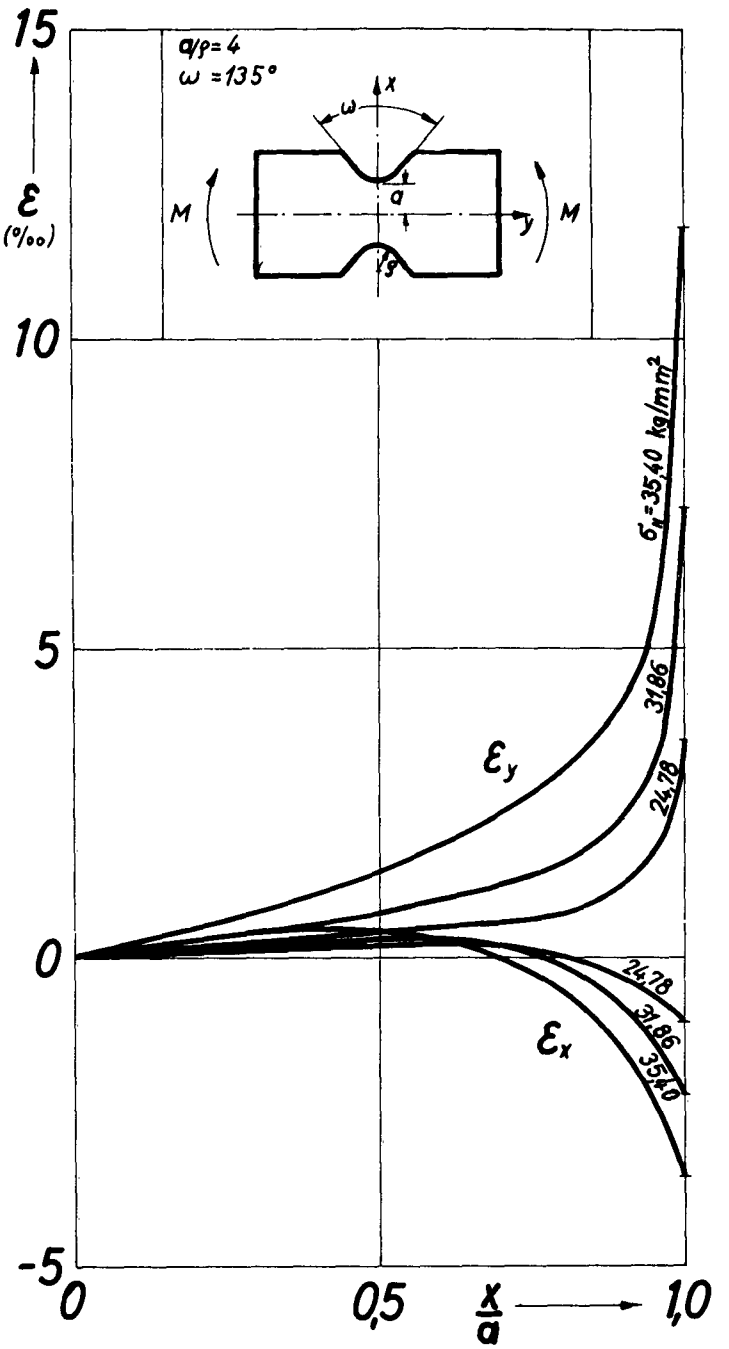

Fig.26 Strain-distribution over the minimum section of a double-notched bending-bar, $a/\rho = 4$, $\omega = 135°$ for various σ_N (Material Steel St.00.21, plastic range)

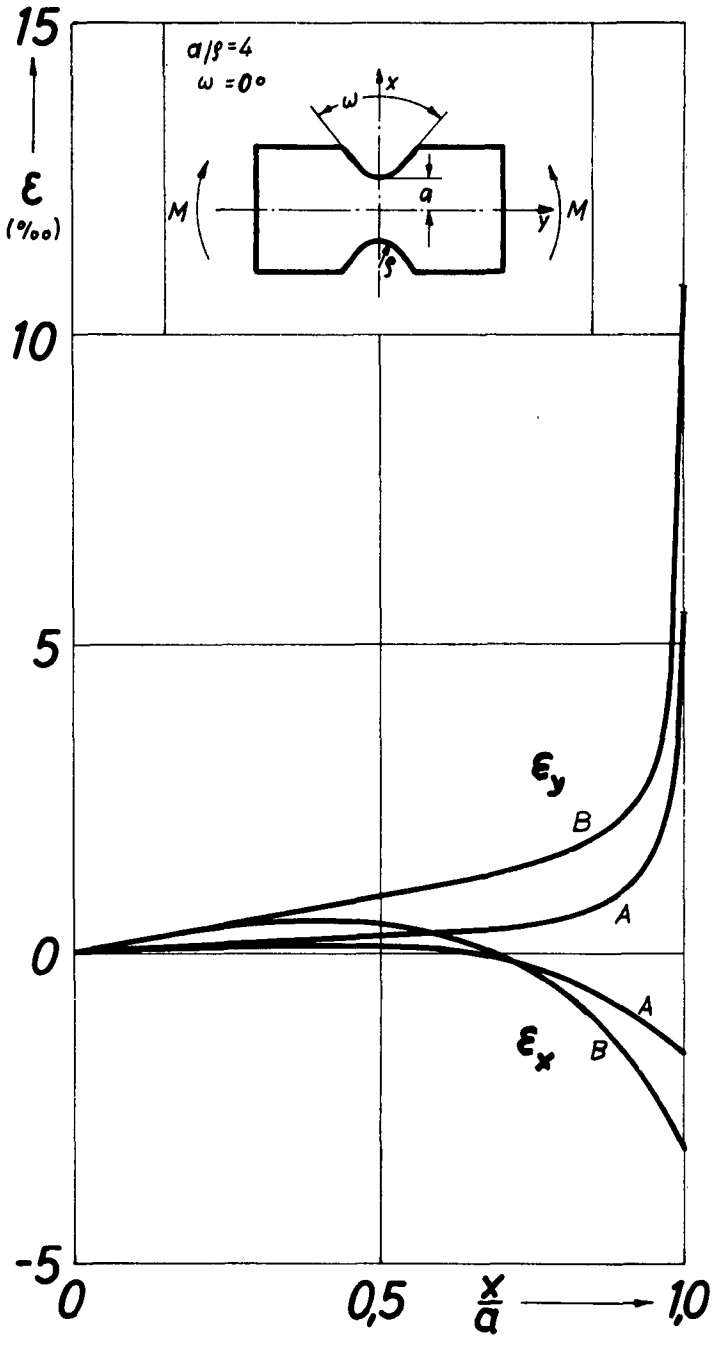

Fig.27 Distribution of the remaining strains over the minimum section of a double-notched bending-bar ($a/\rho = 4$, $\omega = 0^{\circ}$; material Steel St.00.21)

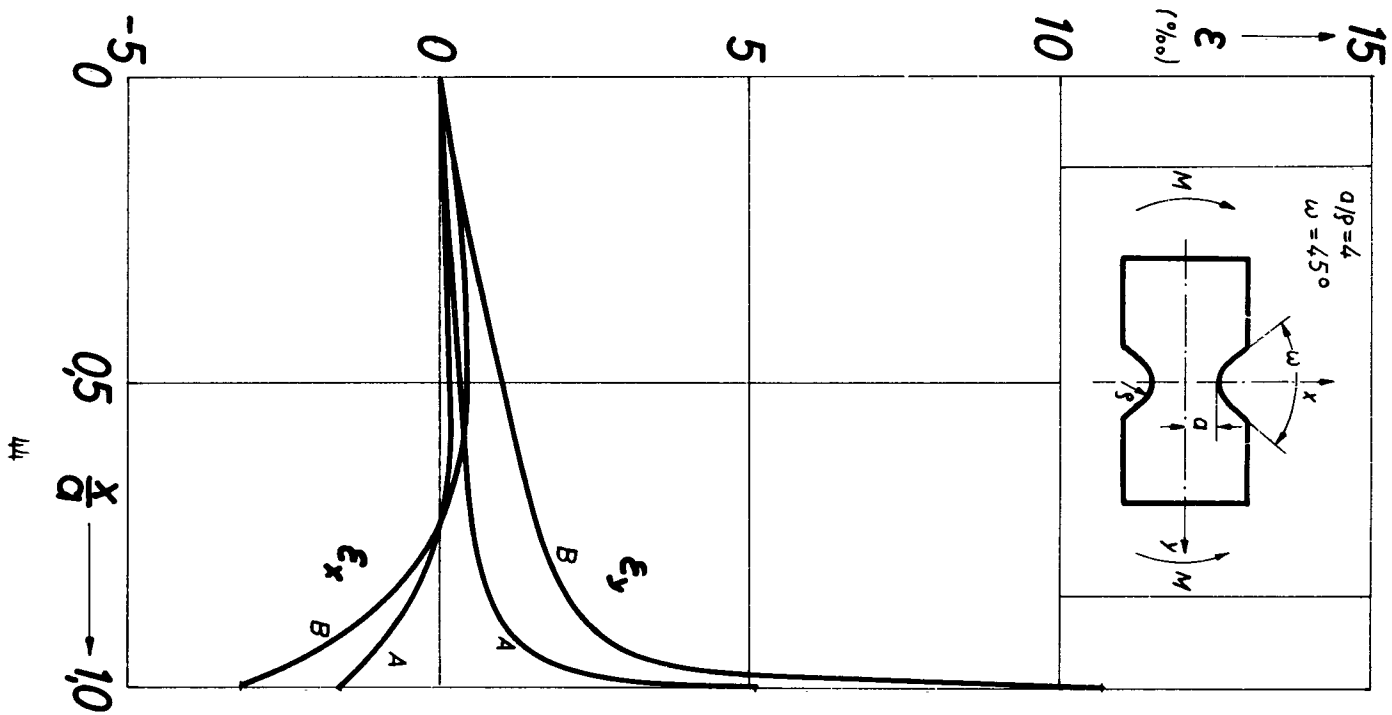

Fig.28 Distribution of the remaining strains over the minimum section of a double-notched bending-bar ($a/\rho = 4$, $\omega = 45^{\circ}$, material Steel St.00.21)

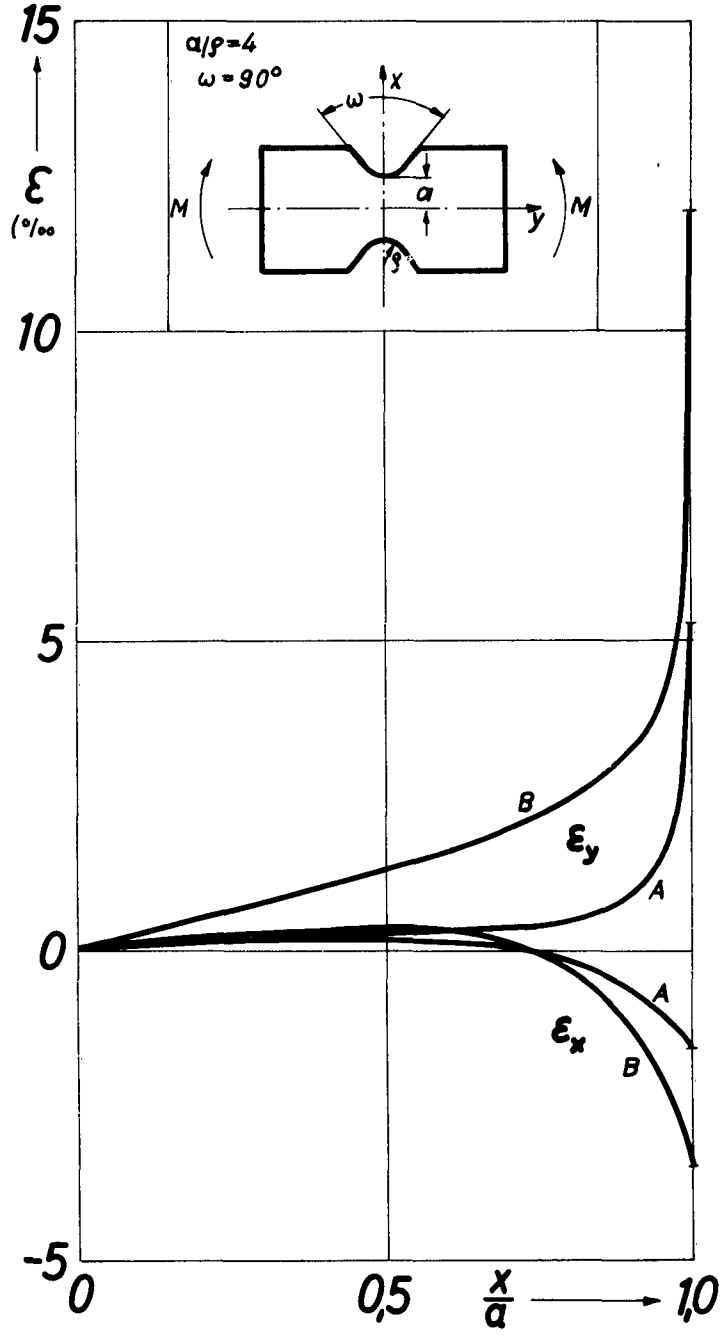

Fig.29 Distribution of the remaining strains over the minimum section of a double-notched bending-bar ($a/\rho = 4$, $\omega = 90°$; material Steel St.00.21)

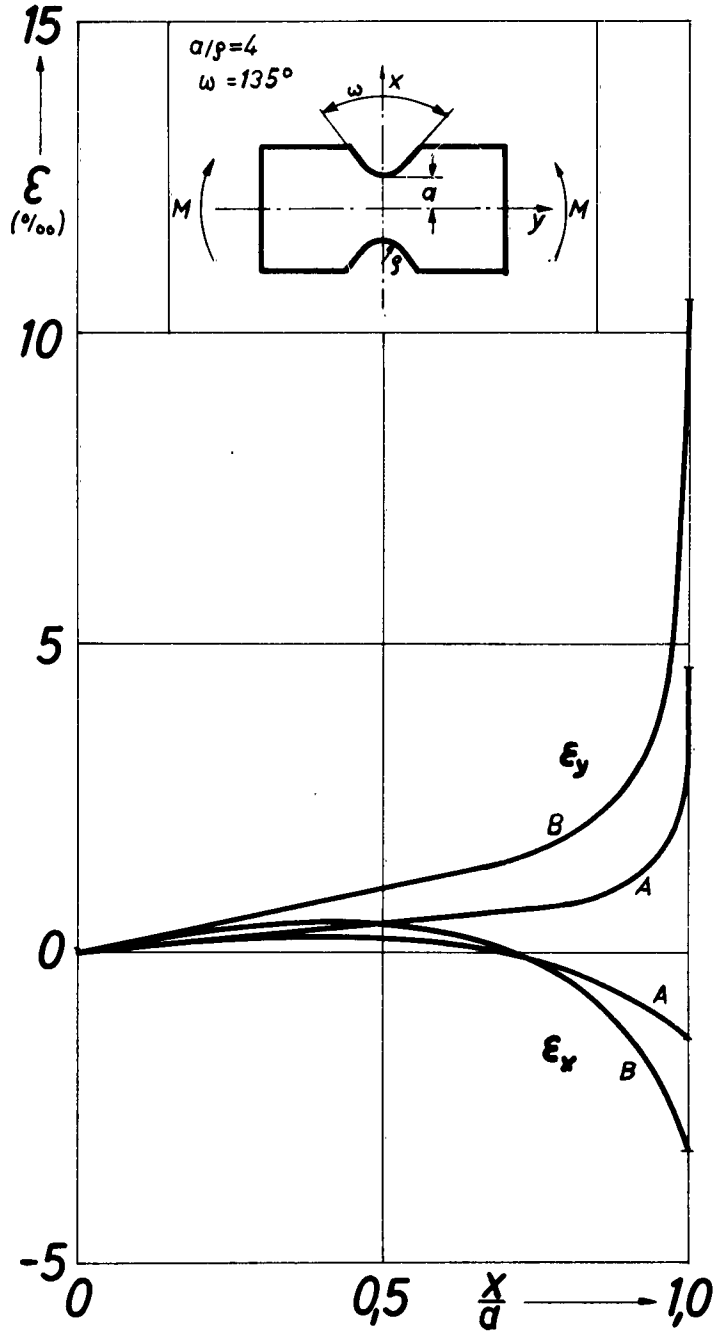

Fig.30 Distribution of the remaining strains over the minimum section of a double-notched bending-bar ($a/\varrho = 4$, $\omega = 135°$; material Steel St.00.21)

Fig.31 Isochromatic pattern for a tension bar with shoulder fillet ($a/\rho = 4$) at $\sigma_N = 45$ kg/mm^2 (Material "Velodur")

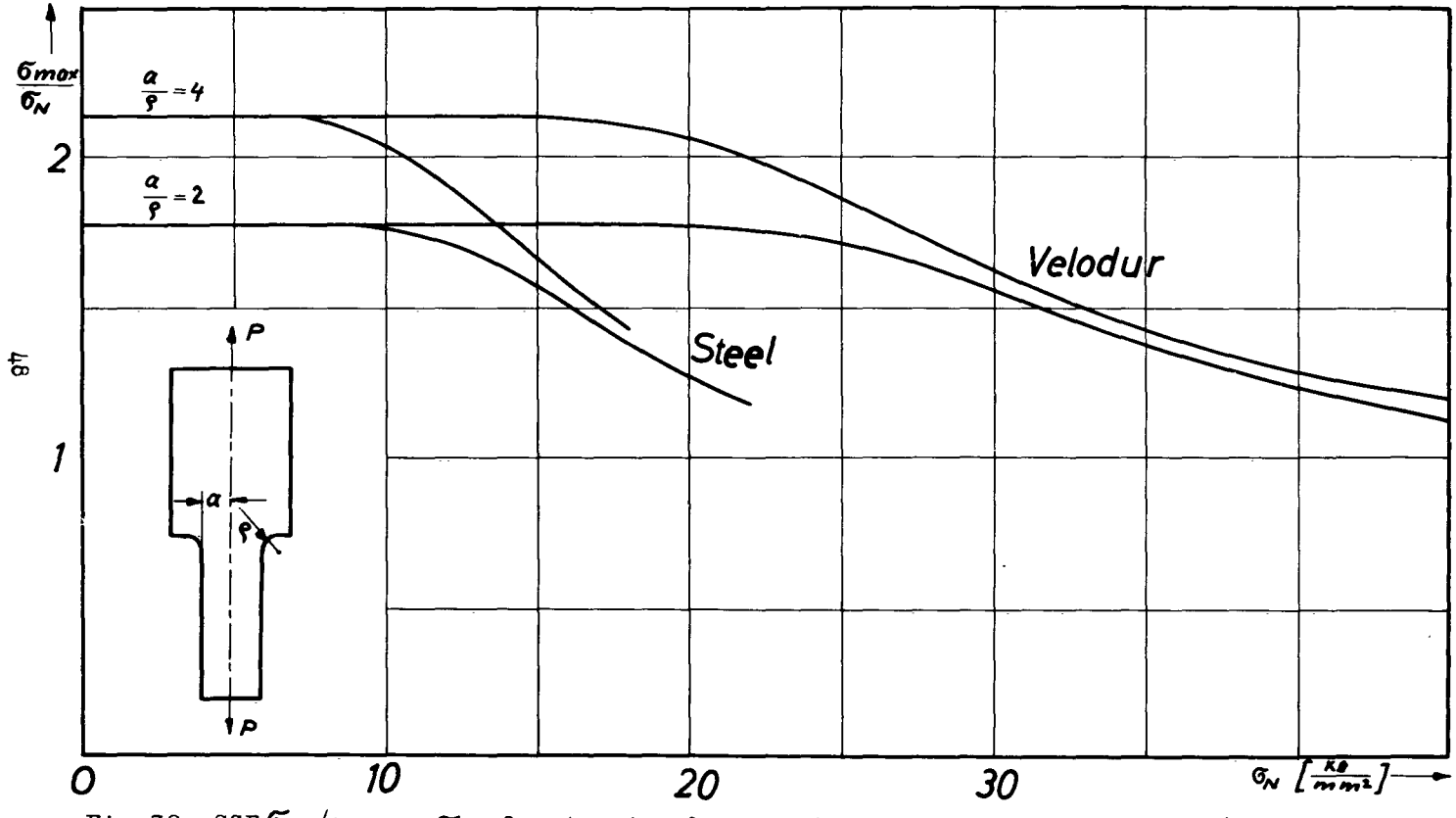

Fig.32 SCF σ_{max}/σ_N vs. σ_N for tension bars with shoulder-fillets with a/ρ = 2 and a/ρ = 4 (Materials: "Velodur" and Steel St.00.12)

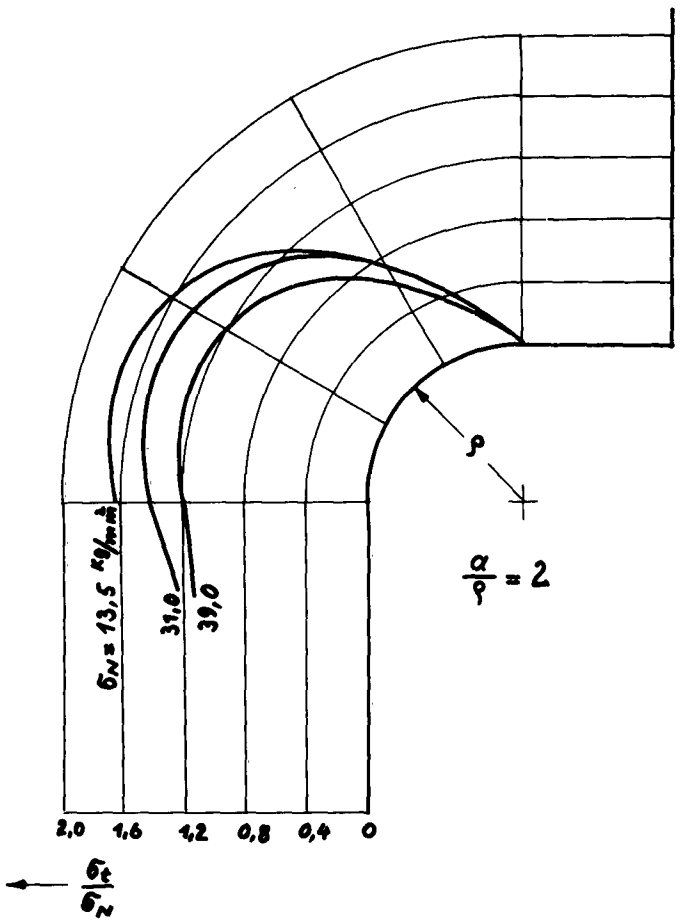

Fig.33 Stress distribution along the edge of a tension bar with shoulder fillet ($\alpha/\rho = 2$) for various σ_N (Material: "Velodur", plastic range)

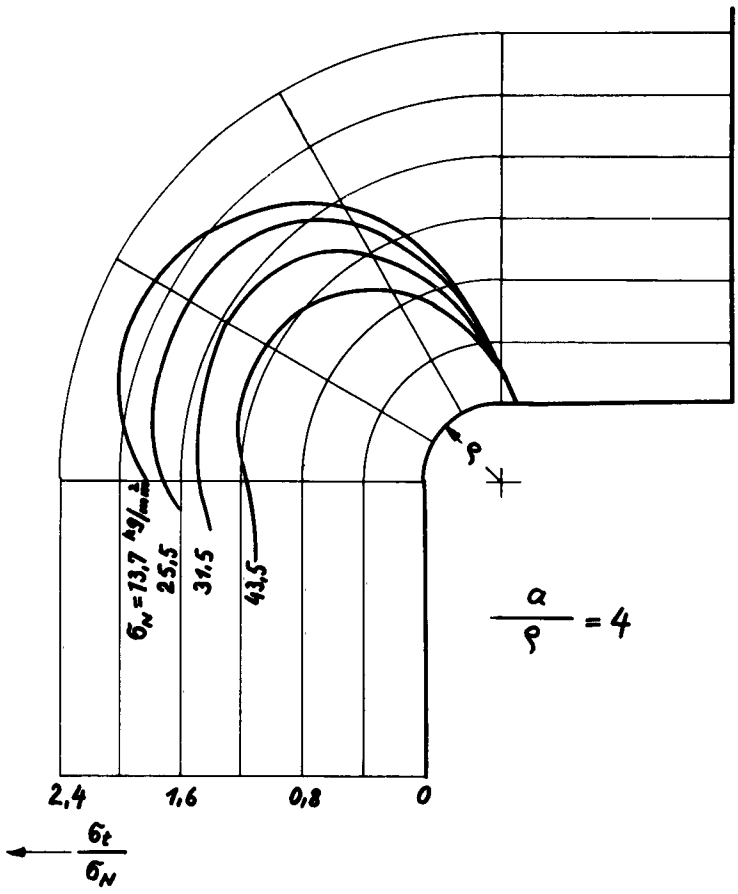

Fig.34 Stress distribution along the edge of a tension bar with shoulder fillet ($a/\rho = 4$) for various σ_N (Material: "Velodur", plastic range)

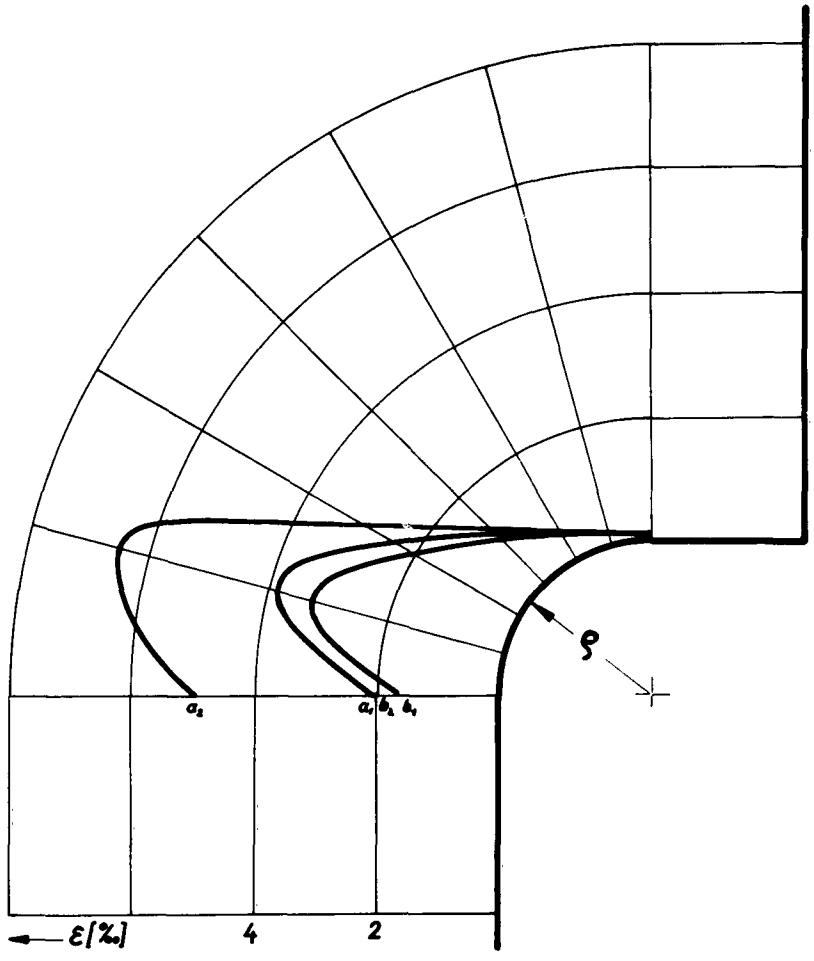

Fig.35 Distribution of the remaining strains along the edge of a tension bar with shoulder fillet with $a/\rho = 2$ (Material "Velodur")

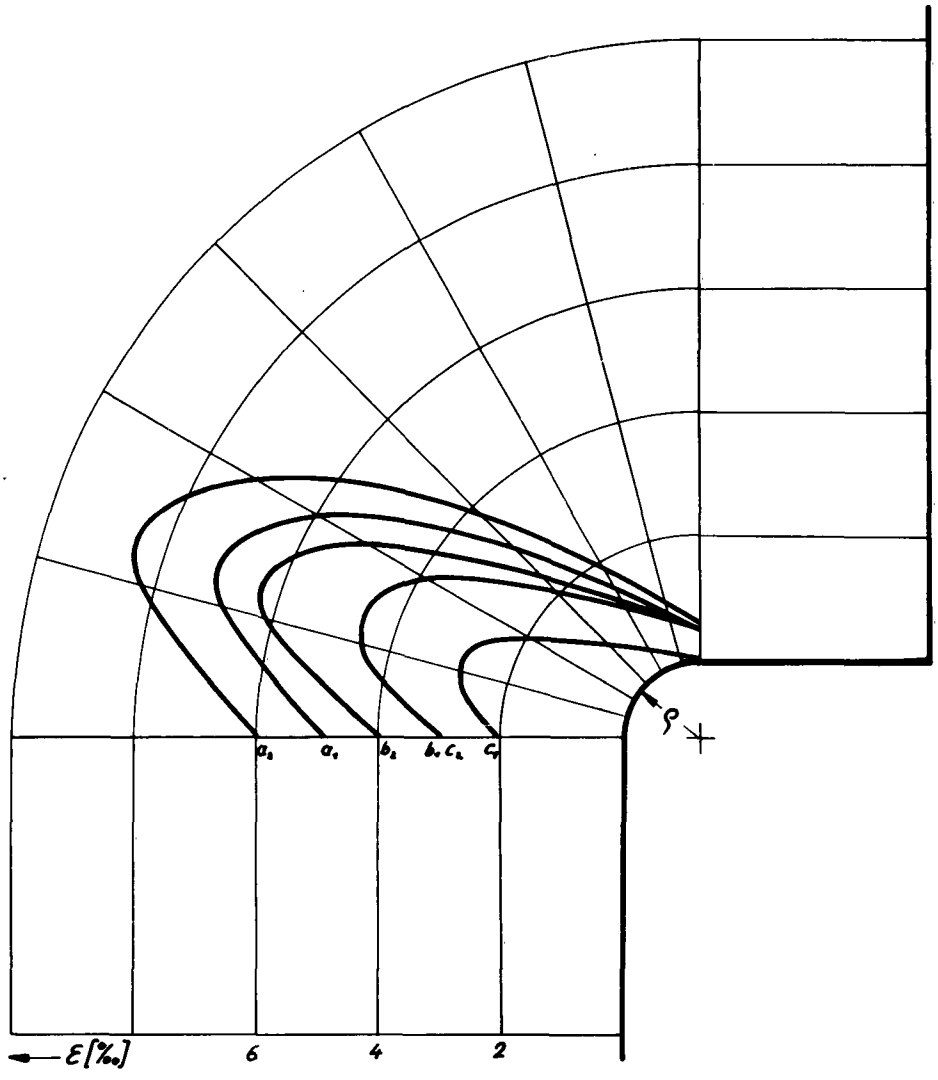

Fig.36 Distribution of the remaining strains along the edge of a tension bar with shoulder fillet with $a/\rho = 4$ (Material "Velodur")

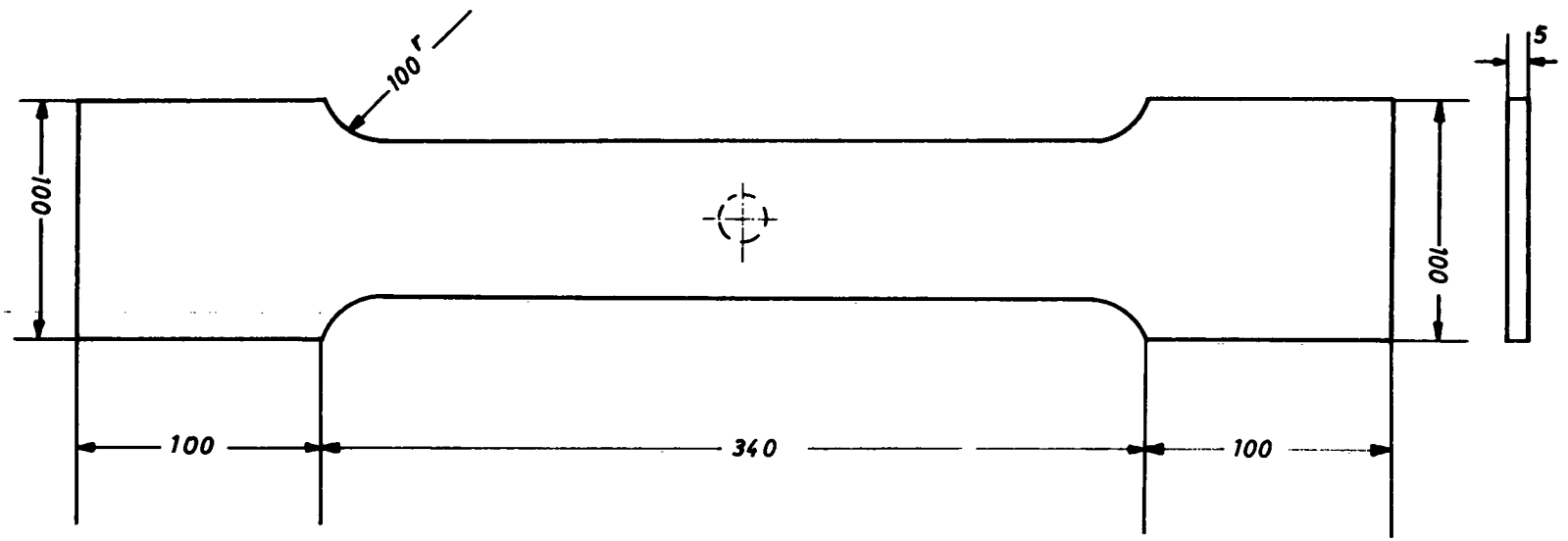

Fig.37 Specimen shape and dimensions in mm for fatigue tests

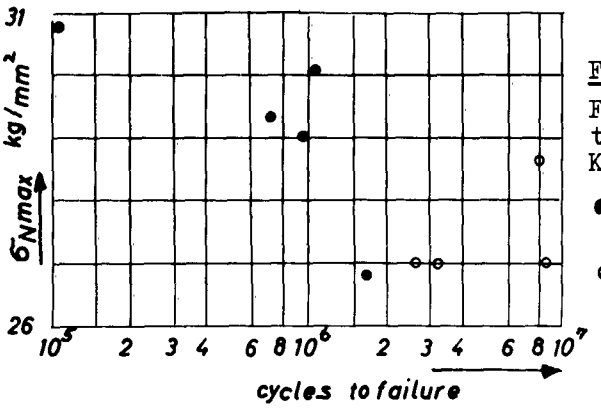

Fig.38

Fatigue test results for the unnotched specimens, K = 0

- ● specimens which failed
- o specimens which did not fail

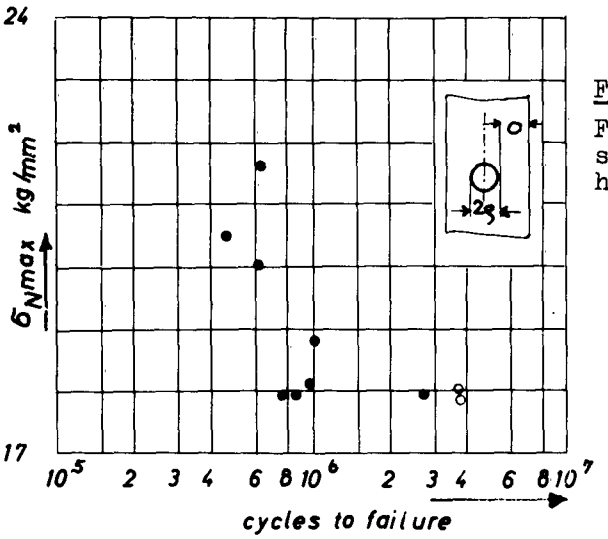

Fig.39

Fatigue test results for specimens with central hole ($a/\varrho = 3$), K = 0

- ● specimens which failed
- o specimens which did not fail

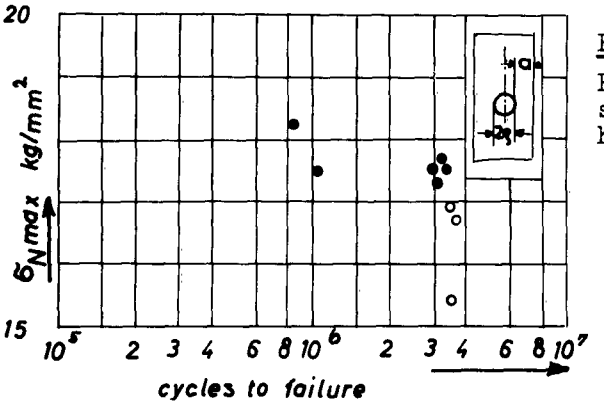

Fig.40

Fatigue test results for specimens with central hole ($a/\varrho = 4$), K = 0

- ● specimens which failed
- o specimens which did not fail

Aeronautical Systems Division, Dir/Materials and Processes, Metals and Ceramics Lab, Wright-Patterson AFB, Ohio.
Rpt No. ASD-TDR-63-361. INVESTIGATION OF THE DISTRIBUTION OF TENSION IN NOTCHED CONSTRUCTION ELEMENTS. Final report, May 63, 54pp. incl illus., 2 refs.

Unclassified Report

The theoretical part of the research work concerns a new treatment of stress- and strain concentrations for a special non-linear deformation law for shear. A relation is obtained by which the real notch stress can be evaluated from the nominal stress and the elastic stress concentration factor. The notch-angle is exactly taken into account.

The experimental part contains static and fatigue tests with variously notched specimens. The strain-measurements were performed by electrical strain gages; additional measurements were made by means of the photoelastic stress-coat method. The aim of the static tests was the investigation of the notch-angle influence on the elastic stress concentration factor for tension and bending, the determination of the stress- and strain distribution in the elastic and plastic range, respectively, and also the dependence of the stress concentration factor on the nominal stress for the materials used (Steel St.00.12, St.00.21, Aluminum alloy "Velodur"). The result of the fatigue tests was the establishment of Wöhler-curves for two different specimen shapes (bars with central holes) and their comparison with the Wöhler-curve of the corresponding unnotched specimen.

(over)

1. Mechanical properties
2. Physics
3. Aluminum alloys
4. Stainless steel
I. AFSC Project 7351, Task 735106
II. Contract No. AF 61(052)-200
III. Technische Hochschule, Munchen, Germany
IV. Dr. -Ing. H. Neuber
V. Aval fr OTS
VI. In ASTIA collection

Aeronautical Systems Division, Dir/Materials and Processes, Metals and Ceramics Lab, Wright-Patterson AFB, Ohio.
Rpt No. ASD-TDR-63-361. INVESTIGATION OF THE DISTRIBUTION OF TENSION IN NOTCHED CONSTRUCTION ELEMENTS. Final report, May 63, 54pp. incl illus., 2 refs.

Unclassified Report

The theoretical part of the research work concerns a new treatment of stress- and strain concentrations for a special non-linear deformation law for shear. A relation is obtained by which the real notch stress can be evaluated from the nominal stress and the elastic stress concentration factor. The notch-angle is exactly taken into account.

The experimental part contains static and fatigue tests with variously notched specimens. The strain-measurements were performed by electrical strain gages; additional measurements were made by means of the photoelastic stress-coat method. The aim of the static tests was the investigation of the notch-angle influence on the elastic stress concentration factor for tension and bending, the determination of the stress- and strain distribution in the elastic and plastic range, respectively, and also the dependence of the stress concentration factor on the nominal stress for the materials used (Steel St.00.12, St.00.21, Aluminum alloy "Velodur"). The result of the fatigue tests was the establishment of Wöhler-curves for two different specimen shapes (bars with central holes) and their comparison with the Wöhler-curve of the corresponding unnotched specimen.

(over)

1. Mechanical properties
2. Physics
3. Aluminum alloys
4. Stainless steel
I. AFSC Project 7351, Task 735106
II. Contract No. AF 61(052)-200
III. Technische Hochschule, Munchen, Germany
IV. Dr. -Ing. H. Neuber
V. Aval fr OTS
VI. In ASTIA collection